RSC Advances

PAPER

View Article Online
View Journal | View Issue

Cite this: *RSC Adv.*, 2025, **15**, 10671

Machine learning tools for the characterization of bioactive metabolites derived from different parts of *Ochrosia elliptica* Labill. for the management of Alzheimer's disease†

Mohamed A. Salem,‡[a] Essam Abdel-Sattar,*[b] Asmaa A. Mandour*[c] and Riham A. El-Shiekh[b]

Currently, natural products are one of the most valuable resources for discovering novel chemical medicinal entities. A total of 41 compounds were tentatively identified from the stems, barks, roots, and fruits of *Ochrosia elliptica* Labill. using UPLC-MS/MS analysis. The binding affinities of these biomarkers for the active sites of acetyl- and butyryl-cholinesterase enzymes were further validated using molecular docking studies, which showed good results with (−)C-Docker interaction energy ranges of 30.17–86.73 and 26.81–72.42 (kcal mol^{-1}), respectively. The most active predicted compound was a quercetin derivative [quercetin-3-*O*-rhamnosyl-(1-3)-rhamnosyl-(1-6)-hexoside, E = −86.73, −72.42 kcal mol^{-1}], which was subjected to dynamic simulation studies against the two enzymes to investigate the stability of the docked conformation. Root-mean-square fluctuations (RMSFs) showed values of 0.25–4.0 and 0.50–4.75 compared to free-state protein RMSF values of 0.25–4.5 and 0.5–7.5, revealing stable fluctuations over time after docking of this compound to AChE and BChE active pockets, respectively. AI in pharmacology can significantly improve patient outcomes and advance healthcare. Ligand binding or catalytic sites for AzrBmH21, AzrBmH22/3, and AzrBmH24/5 were predicted using a machine learning algorithm based on the Prank Web and DeepSite chemoinformatics tools. These findings will establish a scientific foundation for further investigations into the *Ochrosia* genus, particularly in relation to Alzheimer's disease.

Received 2nd January 2025
Accepted 26th February 2025

DOI: 10.1039/d5ra00021a

rsc.li/rsc-advances

1 Introduction

Alzheimer's disease (AD) is a neurological condition that impairs judgement, thinking, orientation, and cognitive functions.[1–4] One in every 85 people worldwide is predicted to have AD by 2050 owing to the disease's increasing prevalence in the elderly population.[5,6] The disease's pathogenic features include the absence of the essential neurotransmitter acetylcholine (ACh), the build-up of amyloid plaques (Aβ), the formation of neurofibrillary tangles (NFTs), and nerve damage due to oxidative stress.[7] Research is now focused on the development of cholinesterase inhibitors that can reinstate ACh activity, antioxidants, anti-amyloid, and anti-inflammatory medications.[8–10]

Regretfully, the FDA has only approved few medications, including galantamine, donepezil, and rivastigmine for the treatment of AD. These medications work by raising the brain's ACh levels. However, these medications exhibit a poor efficacy rate and serious adverse effects, including hepatotoxicity.[11,12] According to published research, there are about 189 medications that are licensed for use in clinical settings that are derived from plant sources,[12–15] reducing the risk of certain chronic illnesses such as neurodegenerative conditions, especially AD.[16]

The genus *Ochrosia* (Apocynaceae) has approximately 39 species of trees that grow naturally in tropical or subtropical Malaysia and west of the Pacific Islands.[17,18] Phytochemical investigations on plants in this genus resulted in the identification of distinct skeletal types of indole alkaloids with anticancer properties, which piqued the interest of pharmacologists.[19] *O. elliptica* Labill. is primarily recognized for the ellipticine series of indole alkaloids, as well as lignans,

[a]*Department of Pharmacognosy and Natural Products, Faculty of Pharmacy, Menoufia University, Gamal Abd El Nasr St, Shibin Elkom, 32511, Menoufia, Egypt. E-mail: mohamed.salem@phrm.menofia.edu.eg*

[b]*Pharmacognosy Department, Faculty of Pharmacy, Cairo University, Kasr El Aini St, P. B. 11562, Cairo, Egypt. E-mail: Riham.adel@pharma.cu.edu.eg; essam.abdelsattar@pharma.cu.edu.eg*

[c]*Pharmaceutical Chemistry Department, Faculty of Pharmacy, Future University in Egypt (FUE), Cairo 11835, Egypt. E-mail: asmaa.abdelkereim@fue.edu.eg*

† Electronic supplementary information (ESI) available. See DOI: https://doi.org/10.1039/d5ra00021a

‡ Current address: The BioActives Lab, Biological and Environmental Science and Engineering Division (BESE), King Abdullah University of Science and Technology (KAUST), Thuwal 23955-6900, Saudi Arabia.

coumarins, and phenolic acids.[19–22] Previously studied biological activities were primarily involved in the cytotoxic attributes of ellipticine. Ellipticine and its derivatives largely impede cell cycle progression and trigger apoptotic pathways in various cancer cell types.[23]

The integration of machine learning (ML) into natural product research is revolutionizing drug discovery by addressing traditional challenges and unlocking new opportunities.[24,25] The increasing trend of using ML in natural product research and drug discovery is reshaping the pharmaceutical landscape. ML algorithms can analyze large datasets swiftly, identify promising compounds, predict drug–target interactions, and optimize drug development processes. This integration is making drug discovery more efficient, accurate, and cost-effective, ultimately accelerating the development of new and innovative treatments. It is an exciting advancement that holds great potential for the future of medicine and healthcare.

Metabolomics is a valuable method for thoroughly analyzing and comparing metabolites in biological systems.[26] Metabolomics has proven to be a useful method, especially for plants, where thousands of undiscovered metabolites occur in substantial variety and numbers.[27] The untargeted approach helps researchers better understand the complexity of these mixtures by offering an objective technique for comparing metabolite profiles between groups.[28] It may also aid in understanding which metabolites are most important for specific pharmacological activities.[29] Previous metabolomic techniques, particularly liquid chromatography-tandem mass spectroscopy (LC-MS/MS)-based metabolomics, focused on specific groups of substances such as alkaloids from the Apocynaceae family.[30–32]

Molecular docking and molecular dynamics simulation can improve our understanding of protein–ligand interactions. Furthermore, it has proven to be quite precise in screening bioactive components against a wide range of targets. It saves scientists' time, effort, and budget during the lengthy drug discovery process.[33,34] Docking, in particular, can be utilized to anticipate new therapeutic drugs capable of treating a variety of chronic diseases.[35,36] AI-based prediction models are being developed to address these challenges, and they may play a role in future screening, diagnosis, treatment selection, and salvage therapy decisions.[37]

The cholinesterases, which include acetylcholinesterase (AChE, EC 3.1.1.7) and butyrylcholinesterase (BChE, EC 3.1.1.8), are a family of esterases that catalyze the hydrolysis of cholinergic neurotransmitters into choline and their corresponding acids, resulting in the resumption of the activated cholinergic neuron to its state of rest.[38] AChE is considered a high-performance cholinesterase with highly specific catalytic activity towards ACh (80%), whereas BChE, a replacement for AChE, is a non-selective cholinesterase that can breakdown both ACh and butyrylcholine.[39] Previous research has shown that ACh depletion can produce a variety of neurological abnormalities in the brain's cortical cholinergic locations in AD patients. Several pharmacotherapeutics acting as acetylcholinesterase inhibitors (AChEIs) have been found to increase the concentration of Ach, and hence, contribute to the relief of the symptoms of AD.[40]

As a part of our ongoing research into phytochemically and biologically interesting medicinal plants,[41–45] this study aimed to use a metabolite profiling strategy for understanding the chemical profiles of the stems, barks, roots, and fruits of *O. elliptica* Labill., correlating them with their anti-cholinesterase activities (AChE and BChE inhibitory activities) for the first time. Our study will be the first metabolite profiling record of *O. elliptica* Labill. identifying all metabolites in a single run. Furthermore, molecular docking simulations were utilized to investigate the potential binding mechanisms and intermolecular interactions of the discovered compounds with AChE and BChE active sites. These findings may be the first to show that this genus and its identified metabolites have multi-targeted potential against AD.

2 Material and methods

2.1. Plant materials

The stems, barks, roots, and fruits of *Ochrosia elliptica* Labill. were collected in December 2022 from the Experimental Station of the Faculty of Pharmacy, Cairo University, Giza, Egypt. The plant was authenticated by Mrs Therese Labib, Consultant of Plant Taxonomy at the Ministry of Agriculture and the Former Director of El-Orman Botanical Garden. A voucher with specimen no. (28.12.2012) was deposited at the herbarium of the Pharmacognosy Department, Faculty of Pharmacy, Cairo University.

2.2. Preparation of the samples

The air-dried samples (200 g) were extracted separately with 70% ethanol (3× 350 mL) till exhaustion. Solvents were removed using a rotary evaporator at 60 °C to obtain the extracts, after that 10 mg from each extract was moved to an LC vial, dissolved in 1.5 mL methanol, and kept at −20 °C till further LC-MS analysis. For each sample, three replicates were extracted in parallel under the same conditions. To conduct biological analysis, 5 mg of dried methanolic extracts were dissolved in methanol.

2.3. Chemicals

Tris–HCl buffer, dithio-bis-(2-nitrobenzoic acid) (DTNB), butyrylthiocholine iodide, acetylthiocholine, acetylcholinesterase (AChE) from electric eel, and butyrylcholinesterase (BChE) from horse serum were supplied by Sigma Chemical Co. (St. Louis, MO, USA).

2.4. UPLC-MS/MS chemical profiling and metabolite annotations

Aliquots of the samples (1 mg of the methanol extract) were resuspended in 1 mL of LC-grade 50% methanol in water, samples were quickly vortexed, sonicated for 3 min and finally centrifuged at 14 000 rpm for 5 min adopting the conditions mentioned previously.[46] The metabolites resulting from the tested extracts were separated using an RP High Strength Silica

(HSS) T3 C18 column (100 mm × 2.1 mm containing 1.8 μm diameter particles) in a Waters UPLC system (Acquity, Waters Corporation, USA), with an injection volume of 3 μL and a flow rate of 0.3 mL min^{-1}. The chromatographic conditions are as follows: mobile phase A (water containing 0.1% formic acid) and mobile phase B (acetonitrile containing 0.1% formic acid). The separation gradient is as follows: 0–1 min at 1% mobile phase B; 1–11 min mobile phase B was increased linearly from 1 to 40%; 11–13 min, mobile phase B was increased linearly from 40 to 70%; 13–15 min, mobile phase B was increased linearly from 70 to 99%; 15–16 min, mobile phase B was maintained at 99%; 16.0–17.0 min, mobile phase B was linearly decreased from 99 to 1%; 17.0–20.0 min, mobile phase B was kept at 1%. The column temperature was 40 °C. Mass spectra were attained using a high-resolution Orbitrap mass analyzer (Q Exactive system, Thermo Fisher Scientific, Waltham, MA, USA). Data acquisition was completed in data-independent acquisition (DIA), which was obtained in the positive mode, with the scanning range from 100 to 1500 *m*/*z*. The ion spray voltage and positive ion voltage were both 3500 V, the negative ion voltage was 3000 V, ion source was Heated Electrospray Ionization (HESI), the sheath gas pressure was 40 psi, the auxiliary heating gas pressure was 15 psi, and the ion source heating temperature was 300 °C. The Thermo X-calibur software (Thermo Scientific, Germany) was used for instrument control, data acquisition and quality checking of the MS/MS data. The raw files were subsequently brought into MSDial for subsequent processing.[47]

2.5. Cholinesterase inhibitory activities determination

The cholinesterase inhibition assays were performed by the Ellman colorimetric method with slight modifications.[4,48] In a total volume of 170 μL of Tris–HCl buffer (0.1 M, pH 8), 20 μL of various extracts in methanol with different concentrations, and 20 μL of enzyme solution containing 1 U mL^{-1} were incubated for 10 min at room temperature. After adding 20 μL of substrate solution and 40 μL of DTNB, the mixture was incubated at room temperature for 15 minutes. The absorbance of the combination was measured at 410 nm using a plate reader (Techan, USA). Donepezil was employed as a positive control. The percentage inhibition of enzyme activity was calculated by comparing with the negative control

$$\text{Inhibtion}\% = \left(\frac{A_0 - A_1}{A_0}\right) \times 100$$

where A_0 is the absorbance of the negative control (enzyme without samples) and A_1 is the absorbance of the enzyme with the tested samples. Assays were carried out in triplicate. To calculate the IC_{50} values, each sample was assayed at 5 concentrations (200, 100, 50, 10, and 5 μg mL^{-1}). The IC_{50} values were obtained from the dose–effect curves by linear regression.

2.6. Molecular modeling

2.6.1. Protein and ligand preparation. The two crystal structures of human acetylcholinesterase, AChE (in complex with donepezil ligand) (PDB ID: 7E3H)[49] and human butyrylcholinesterase, BChE (in complex with *N*-((1-(2,3-dihydro-1*H*-inden-2-yl)piperidin-3-yl)methyl)-*N*-(2-methoxyethyl)-2-naphthamide ligand) (PDB ID: 4TPK)[50] were successfully downloaded from the Protein Data Bank (**https://www.rcsb.org/**).[51,52]

Further, the 2D chemical structures of forty-one compounds were first sketched using ChemBioDraw Ultra 14.00 (Cambridge Soft Corp., Cambridge, MA) and then converted into three-dimensional (3D) structures using Discovery Studio (DS 4.0 Biovia Discovery Studio 2016 64-bit Client). Simulation for the ligands was carried out by applying CHARMm Forcefield with partial charge MMFF94 for ligand preparation.

2.6.2. Ligand binding site prediction. Two machine learning algorithms were adopted to predict the ligand binding sites on the two protein targets of interest, namely AChE (PDB ID: 7E3H) and BChE (PDB ID: 4TPK). The 3D structures of the two potential targets were analyzed using PrankWeb and DeepSite web servers in order to identify the available pockets for small molecule binding, based on the sequence information of the protein 3D structure.[53] Visual analysis was also applied to investigate the most reliable binding pocket through the identification of the essential amino acids within each pocket compared to the pocket score and probability score results, putting into consideration the number of amino acids in each pocket. This was achieved *via* uploading the 3D structure of each of the two targets using their PDB ID to both PrankWeb and DeepSite web servers for analysis.[54]

To reconfirm the previously predicted catalytic amino acids of the active pockets of the two mentioned proteins, CAVER Web 1.0 tools (**https://loschmidt.chemi.muni.cz/caverweb/**) was employed for quantum tunneling that played an important role in ligands' dimension determination to investigate the fitting level of the ligand and predict its biological effect.[54]

2.6.3. Molecular docking study. A molecular docking procedure was applied using the Discovery Studio 4.0 Software. All molecular simulations were conducted adopting the C-Docker protocol on the forty-one tested compounds. The two targets studied were subjected to clean protein to complete the missing residues. Moreover, hydrogen atom addition was performed. Water molecules and all unnecessary radicals were successfully removed. All simulations were applied using CHARMm Force Field and partial charge MMFF94.[55] The two enzymes were prepared and minimized, then active sites were identified through selecting the downloaded ligands named donepezil and *N*-((1-(2,3-dihydro-1*H*-inden-2-yl)piperidin-3-yl)methyl)-*N*-(2-methoxyethyl)-2-naphthamide for the two targets: AChE and BChE, respectively. Downloaded ligands were removed from each target prior to their re-docking together with the new compounds after preparation. The selection of the best pose out of the 10 poses for each docked compound was based on the visual inspection of the ranked conformations (according to their C-Docker interaction energy in kcal mol^{-1}, where lower energy values indicated more stable stronger interactions). Data analysis was presented as 2D diagrams of the key molecular interactions necessary for ligand-protein binding, which helped to predict the essential pharmacophoric features of ligands incorporated in hydrogen bonds and hydrophobic

interactions with the essential amino acid residues at the binding pockets of both targets visualized using the Discovery Studio 4.0 and PyMol software.[55,56]

2.6.4. Standard dynamic simulations. Dynamic simulation studies were performed using the Discovery Studio 4.0 software against the two downloaded targets: AChE (PDB ID: 7E3H) and BChE (PDB ID: 4TPK). Studies were carried out on the docked forms of enzymes and compared to their free protein state. Standard dynamic cascades was applied keeping the first minimization algorithm adjusted to the steepest descent enabling 2000 maximum steps and Root Mean Square (RMS) gradient 1.0. The second minimization algorithm was set to a conjugate gradient with 2000 maximum steps and the RMS gradient equals 0.1. The heating phase was of a simulation time of 4 Ps keeping a 2 Ps interval. The initial temperature of 50 and a target temperature of 300 with a maximum velocity of 2000 were adjusted. The equilibration phase of simulation time of 20 Ps and interval of 2 Ps was performed keeping a target temperature of 300 with a maximum velocity of 1000. For the implicit solvent model with the Leapfrog Verlet dynamics integrator protocol, generalized born with simple switching was adjusted.[57,58] The other details are shown in Fig. S1–S5.†

3 Results and discussion

3.1. UPLC-MS/MS chemical profiling and metabolite annotations

The LC-ESI-MS/MS approach is presented for profiling phytocompounds in the tested plant extracts. Furthermore, the fragmentation patterns found in the mass spectrum helped the annotation of these molecules. Compounds were identified by comparing their retention times and distinctive MS spectrum data to those from the reference literature. The combination of UHPLC's superior chromatographic resolution and separation capabilities with HR-MS allows for structural annotations based on accurate mass measurement in both MS and MS–MS investigations. These approaches provide a substantial advantage for screening target chemicals from complicated matrices. *O. elliptica* contains a high concentration of alkaloids.[18] Alkaloid-bearing plants were detected in positive ion mode, with 39 chemicals found in various organs. In addition, two quercetin derivatives were identified, bringing the total number of 41 compounds detected in positive ionization mode (see Table 1, Fig. 1, and S6†). Representative compounds with fragmentation patterns are illustrated in the respective paragraphs.

Compounds **1**, **4**, **23**, and **26** are types of indole alkaloids identified as yohimbine and its derivatives. The MS spectra of yohimbine showed a protonated ion at *m*/*z* 355.2018 $[M + H]^+$ and MS/MS showed ions at *m*/*z* 117, 144, 162, 180, 194, 212, and 224, and the most abundant ion was found at *m*/*z* 144 and ions at *m*/*z* 214 and *m*/*z* 224 are the other ions showed up with considerable abundance. Ring cleavage at C-2,3 and C-4,5 resulted in the formation of indole derivative with *m*/*z* 144 $[C_{10}H_{10}N^+]$ and *m*/*z* 212 $[C_{11}H_{18}NO_3^+]$. Similarly, ring cleavage at C-2,3 and C-5,6 resulted in the formation of *m*/*z* 224 $[C_{12}H_{18}NO_3^+]$. These three peaks are characteristic peaks for identifying the similar yohimbine type of compound like 10-methoxyyohimbine (**1**), which showed peaks at *m*/*z* 384 (M^+), 383 (M-l), 369 (M-15), 355, 354, 353, 324, 214, 201, 200, 199, 192 (M^{++}), 186, 174, 173, and 153.5. The peaks at *m*/*z* 214, 200, 199, and 186 are the typical yohimbine peaks moved to a value 30 mass units higher because of the presence of the aromatic methoxyl group. 18-Hydroxyepialloyohmbine (**4**) and *O*-acetylyohimbine (**23**) are identified in the same pattern.

Compounds **2** and **11**: ajmaline and norajmaline are other types of indole alkaloids, showing protonated ions at *m*/*z* 327.2065, and 313.1907 $[M + H]^+$, respectively, and ions at *m*/*z* 131, 144, 158, 182, 194, 210, 220, and 239. *N*-Methyl indole derivative (*m*/*z* 158) is formed by ring cleavage at C-2,3 and C-4,5, and further loss of methyl group from nitrogen atom yields the base peak at *m*/*z* 144 $[C_{10}H_{10}N^+]$. The loss of C_8H_7NO from protonated ions gives *m*/*z* 194 $[C_{12}H_{20}NO^+]$ and cleavage at C-2,3 and C-4,5 from *m*/*z* 194 yields *m*/*z* 108 $[C_7H_{10}N^+]$.

Compound **5**: 10,11-dimethoxyajmalicinine showed protonated ions at *m*/*z* 431.2178 and ions at *m*/*z* 117, 144, 178, 212, 222, and 252. The fragmentation behavior of ajmalicine is similar to that of yohimbine, except the presence of double bond (C-16, 17), oxygen atom in ring D, and methyl group at C-19 position.

Compounds **32**, **33**, **35**, **36**, and **38** are types of indole alkaloids identified as ellipticine and its derivatives showed molecular ion peaks at *m*/*z* 281.16507, 251.1545, 247.1229, 277.1334, 409.17593, and 279.1857, respectively, and characteristic fragment ions at 246 and 247.

Compounds **40** and **41**: reserpine and dehydro-reserpine are trimethoxybenzoic acid-substituted alkaloids, with protonated ions $[M + H]^+$ at *m*/*z* 609.2818 and 607.2658, respectively, with fragment ions at *m*/*z* 174, 195, 236, 365, 397, 448, and 577. Neutral loss trimethoxybenzoic acid of $[M + H]^+$ resulted in the formation of *m*/*z* 397 $[C_{23}H_{29}N_2O_4^+]$. The loss of a hydroxyl group from trimethoxybenzoic acid resulted in the generation of the most abundant peak at *m*/*z* 195 $[C_{10}H_{11}O_4^+]$. The loss of CH_3OH from *m*/*z* 397 yields an ion at *m*/*z* 365 $[C_{22}H_{25}N_2O_3^+]$. Ring cleaving at C-2, 3, C-4, 5, and C-5, 6 resulted in the formation of *m*/*z* 174 $[C_{11}H_{12}NO^+]$ and *m*/*z* 448 $[C_{23}H_{29}NO_8^+]$. Neutral loss of trimethoxybenzoic acid from *m*/*z* 448 generates *m*/*z* 236 $[C_{13}H_{18}NO_3^+]$.

Compounds **12** and **13**: quercetin-3-*O*-rhamnosyl-(1-3)-rhamnosyl-(1-6)-hexoside and rutin were identified in fruits only with molecular ion peaks at *m*/*z* 757.2184, and 611.16162, respectively. The compounds showed characteristic fragment ions at *m*/*z* 465, and 303 due to loss of sugar moieties.[69,70]

3.2. Biological activities of different parts of *O. elliptica* Labill.

The activity of different samples against Alzheimer activity is summarized in Table 2. Acetyl- and butyrylcholinesterase revealed that the samples investigated had more selectivity index to AChE than BChE. Carbazole alkaloids possess the acetylcholinesterase inhibitory potential by the most widely used method, *i.e.* Ellman's method and also are efficient inhibitors of beta amyloid fibril formation.[71] From the results, it can be concluded that the hydroalcoholic extract of *O. elliptica* fruits exhibited the highest biological activity among the

Table 1 Tentatively identified compounds from different organs of *O. elliptica* Labill. using UPLC-MS/MS

Comp no.	RT (min)	Compound name	Exact mass	$[M + H]^+$	Error (ppm)	*O. elliptica* L. Area ($\times 10^6$)				Molecular formula	Mass fragments	Reference
						Stems	Barks	Roots	Fruits			
1	4.93	10-Methoxyyohimbine	384.2049	385.2122	−0.14	25 200	18 500	26 900	18 900	$C_{22}H_{28}O_4N_2$	383 (M-l), 369 (M-15), 214, 199, 192 (M^{++}), 186	59
2	4.99	Ajmaline	326.1994	327.2065	0.169	69.076736	76.689184	17.30335	42.032544	$C_{20}H_{26}O_2N_2$	239, 220, 210, 194, 182, 158, 144	60
3	5.23	10-Hydroxydihydrocorynantheol	314.1994	315.2067	0.081	0.120714	0	5.281832	0	$C_{19}H_{26}O_2N_2$	313, 285, 283 (−2OH), 269, 267, 257, 241, 200, 186, 161, 185 172	61
4	5.25	18-Hydroxyepialloyohimbine	370.1892	371.1967	0.421	4790	10 000	9625.18528	3890	$C_{21}H_{26}N_2O_4$	339, 353, 240, 222, 158, 144	62
5	5.34	10,11-Dimethoxyajmalicinine	430.2103	431.2178	0.248	1.613632	1.86388	4.428456	2.493541	$C_{23}H_{30}N_2O_6$	355, 353, 252, 222, 212, 117, 178, 144	Natural products dictionary
6	5.49	10-Methoxydihydrocorynantheol	328.2150	329.2222	−0.47	111	99.329912	188.719536	26.58068	$C_{20}H_{28}N_2O_2$	313, 299, 297, 283, 281, 255, 214, 200, 199, 186, 168	61
7	5.86	16,22-Dihydro-16-hydroxyapparicine	282.1732	283.1806	0.495	0.524963	0.045075	9.128824	0.171156	$C_{18}H_{22}N_2O$	264 (M-18), 172, 158, 130	63
8	5.93	Corynantheal	294.1732	295.1807	0.678	308	65.234364	1380	663	$C_{19}H_{22}N_2O$	281, 255, 214, 200, 199, 186, 168	61
9	6.09	Reserpinine	382.1892	383.1965	0.068	254	111	169	77.758112	$C_{22}H_{26}N_2O_4$	351, 222, 159, 188, 174	62
10	6.11	Reserpiline	412.1998	413.2076	1.165	77.830664	80.647272	110	32.254536	$C_{23}H_{28}N_2O_5$	397, 323, 222, 218, 204	62
11	6.17	Norajmaline	312.1837	313.1907	−1.228	38.796436	4.932806	6.774066	564	$C_{19}H_{24}N_2O_2$	295, 239, 220, 210, 194, 182, 158, 144, 130	62
12	6.35	Quercetin-3-*O*-rhamnosyl-(1-3)-rhamnosyl-(1-6)-hexoside	756.2112	757.2184	−0.171	10 500	32 500	20 400	6720	$C_{33}H_{40}O_{20}$	609, 465, 303	Natural products dictionary
13	6.70	Rutin	610.1533	611.1616	1.569	29.008288	2.795345	4.912448	676	$C_{27}H_{30}O_{16}$	465, 303	Natural products dictionary
14	6.71	Ochropposinine	358.2256	359.2329	0.141	651	1760	1570	496	$C_{21}H_{30}N_2O_3$	329, 219, 204, 169, 154 (lo), 140, 125	61
15	6.72	Dihydro-reserpiline	414.2154	415.2231	0.871	10.607523	12.781067	10.589717	10.413892	$C_{23}H_{30}O_5N_2$	383, 397, 254, 236, 222, 188, 174, 160	62
16	6.81	10,11-Dimethoxy-19,20-dihydro-16*S*-sitsirikine	416.2311	417.2385	1.47	10.774761	20.76162	18.364846	7.31043	$C_{23}H_{32}N_2O_5$	415, 401, 313, 311, 285, 230	61
17	7.05	3,14-Dihydroellipticine	248.1313	249.1122	0.058	44.865748	1.232219	10.745313	11.298486	$C_{17}H_{16}N_2$	247	Sirus
18	7.12	Ochropamine	366.1943	367.2019	0.846	400	317	579.685248	71.348168	$C_{22}H_{26}N_2O_3$	144, 138, 218, 219, 168	Sirus
19	7.27	Reserpic acid	400.1998	401.2075	0.976	970	775	1640	291	$C_{22}H_{28}N_2O_5$	383, 369, 321, 240, 222, 188, 174	62
20	7.3	Dihydrocorynantheol	298.2045	299.2122	1.237	2440	2490	5580	643	$C_{19}H_{26}N_2O$	283, 281, 255, 214, 200, 199, 186, 168	61
21	7.39	Reserpiline-*N*-oxide	428.1947	429.2027	1.6	874	1500	2340	871	$C_{23}H_{28}N_2O_6$	397, 369, 339, 220, 210, 205, 189, 178, 150	62
22	7.47	Corynantheol	296.1888	297.1964	0.909	113	27.411926	81.495312	15.870396	$C_{19}H_{24}N_2O$	283, 281, 255, 214, 200, 199, 186, 168	61
23	7.48	*O*-Acetylyohimbine	396.2049	397.2111	0.551	328	594	350.388512	171	$C_{23}H_{28}N_2O_4$	338 (M-59, $COOCH_3$), 184, 170, 169, 156	59
24	7.5	*O*-Methyl-vobasinol	368.2099	369.2173	0.137	12 200	16 500	18 000	1600	$C_{22}H_{28}N_2O_3$	353, 326, 297, 265, 281, 222, 174, 144	Natural products dictionary

Table 1 (*Contd.*)

Comp no.	RT (min)	Compound name	Exact mass	$[M + H]^+$	Error (ppm)	*O. elliptica* L. Area ($\times 10^6$)				Molecular formula	Mass fragments	Reference
						Stems	Barks	Roots	Fruits			
25	7.57	3-Dihydrocorynantheol *N*-methosalt	312.2201	313.2274	0.127	77.830664	80.647272	110	32.254536	$C_{20}H_{28}N_2O$	283, 281, 255, 214, 200, 199, 186, 168	61
26	7.59	Yohimbine	354.1943	355.2018	0.622	386	383	285	596	$C_{21}H_{26}N_2O_3$	117, 144, 162, 180, 194, 212, 224	59
27	7.66	Ochroborine B	444.1896	445.1971	0.41	26.964956	54.577132	157.585968	129	$C_{23}H_{28}N_2O_7$	365, 339, 337, 294, 248, 154, 144	64
28	7.93	10,11-Dimethoxypicraphylline	442.2103	443.2180	0.805	205	252	312.399168	99.130208	$C_{24}H_{30}N_2O_6$	413, 368, 317, 281, 279, 240, 204, 154	65
29	8.02	Polyneuridine aldehyde	350.1630	351.1707	1.142	23.164102	217	12.213688	17.48936	$C_{21}H_{22}N_2O_3$	352, 336, 322, 263, 249, 168, 142	66
30	8.19	Holeinine (4-methylreserpiline)	426.2154	427.2230	0.635	51 600	111 000	95 000	32 800	$C_{24}H_{30}N_2O_5$	397, 323, 222, 204, 218	62
31	8.42	Apparicine	264.1626	265.1700	0.32	9830	8100	14 800	1660	$C_{18}H_{20}N_2$	249, 235, 222, 208, 194, 180, 167, 145, 130, 128	67
32	8.43	1,2,3,4-Tetrahydro-9-methoxyellipticine	280.1575	281.1651	0.819	29.7627	76.93712	59.162264	19.478692	$C_{18}H_{20}N_2O$	267, 246	Natural products dictionary
33	8.6	1,2,3,4-Tetrahydroellipticine	250.1469	251.1545	0.816	0.304959	0.649391	209.45456	0.223243	$C_{17}H_{18}N_2$	244	Natural products dictionary
34	8.74	Ochrosamine A	322.1681	323.1756	0.698	2450	3430	2640	455	$C_{20}H_{22}N_2O_2$	255, 219, 149	68
35	8.98	Ellipticine/olivacine	246.1156	247.1229	−0.142	11 200	18 900	6930	5140	$C_{17}H_{14}N_2$	247, 246, 232	Natural products dictionary
36	9.1	9-Methoxyellipticine	276.1262	277.1334	−0.432	23.95127	72.96672	7250	43.883868	$C_{18}H_{16}N_2O$	246, 245	Natural products dictionary
37	9.4	10,11-Dimethoxyalstonine	408.1685	409.1759	0.322	0.379272	0.116939	7.528142	0	$C_{23}H_{24}N_2O_5$	379, 349	Natural products dictionary
38	9.45	1,2-Dihydro-9-methoxyellipticine	278.1419	279.1857	0.554	7.014448	7.858734	2.745834	3.771581	$C_{18}H_{18}N_2O$	246, 245	Natural products dictionary
39	9.69	Serpenticine	378.1579	379.1659	9.69	0.017724	0.055235	3.216962	0.012426	$C_{22}H_{22}N_2O_4$	347, 293, 144	60
40	11.84	Dehydro-reserpine	606.2577	607.2658	1.223	1.40914	1.230805	34.67404	2.777899	$C_{33}H_{38}O_9N_2$	367, 335, 236, 221, 206, 190, 144	62
41	11.88	Reserpine	608.2733	609.2818	1.876	625	1990	6790	265	$C_{33}H_{40}O_9N_2$	577, 448, 436, 397, 365, 236, 195, 174	62

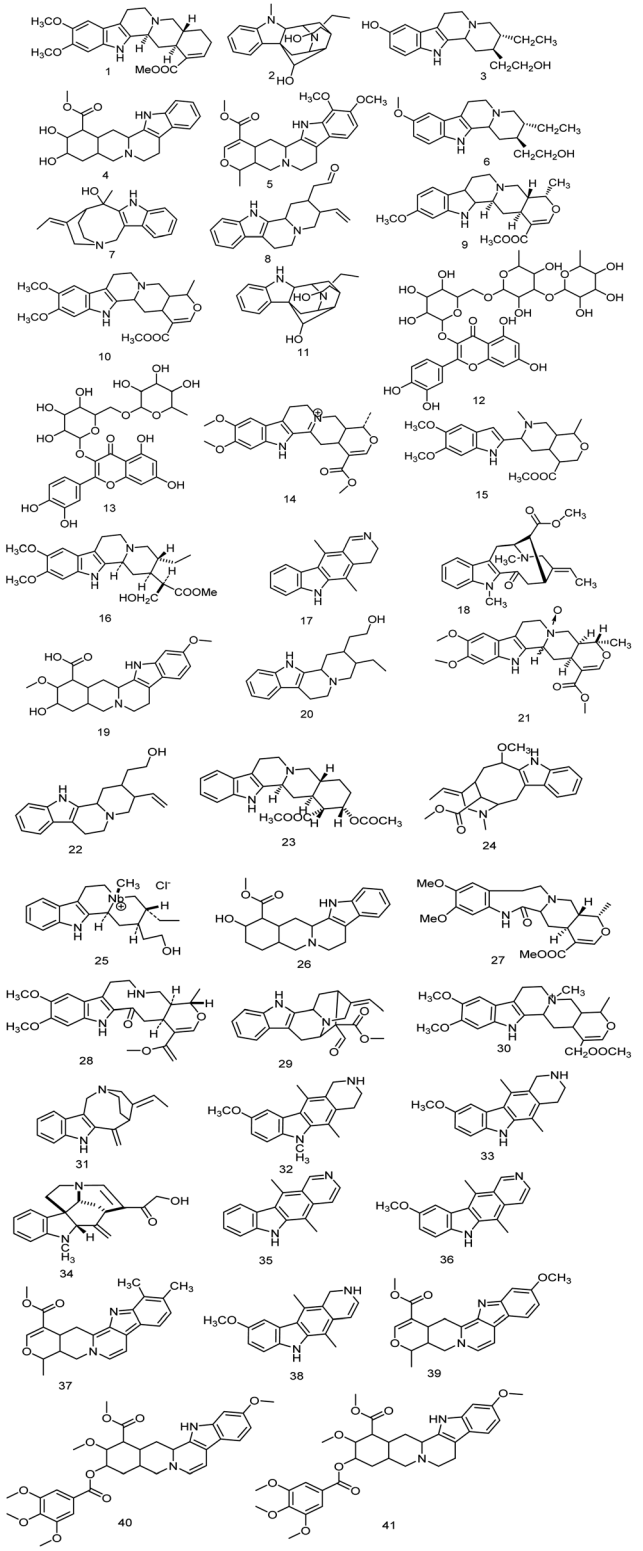

Fig. 1 Structures of the tentatively identified compounds from different organs of *O. elliptica* Labill. using UPLC-MS/MS.

samples studied. This enhanced activity is likely attributed to its rich flavonoid content, as indicated by the UPLC/MS profiling conducted during the research. Phenolics, *i.e.*, flavonoids, are known for their significant therapeutic potential, particularly in nutraceutical applications for AD patients.[72,73] These compounds can be integrated into daily diets to help increase acetylcholine levels and mitigate brain inflammation.[74,75] Incorporating a diet rich in antioxidant and anti-inflammatory flavonoids has been shown to interact beneficially with tau receptors, which may lead to a reduction in gliosis and a decrease in neuroinflammatory markers, as observed in various animal model studies. Such dietary strategies could represent a promising avenue for supporting cognitive health and managing symptoms associated with neurodegenerative conditions.[76] The fruit extract is predominantly characterized by the presence of quercetin derivatives. This specific profile may play a crucial role in the extract's activity as inhibitors of acetylcholinesterase and butyrylcholinesterase. The strong effects of quercetin derivatives suggest that they may be valuable components in developing nutraceuticals due to their antioxidant properties, antibacterial activity, and anti-proliferative effects.[69,70,77] These benefits are particularly relevant for promoting cognitive health and enhancing cholinergic function.[78]

3.3. Molecular modeling studies

3.3.1. Ligand binding site prediction. The two protein targets AChE (PDB ID: 7E3H) and BChE (PDB ID: 4TPK) were subjected to machine learning algorithm based on deep convolutional neural networks: Prank Web and DeepSite chemoinformatics tools, for the prediction of ligand binding sites on the protein structure.[53] Prank Web results are presented as the number of pockets ranked according to the score and probability; the number of residues with their identity and the average conservation score are also available for each pocket per protein. It was observed that the DeepSite web server results appeared generally to be less detailed. It showed the number of pockets per each chain individually, with its score, and the predicted distance to the center of the binding site. Visual inspection was used to identify the surrounding amino acid residues per each pocket.

Table 3 presents the Prank Web prediction results for AChE protein (PDB ID: 7E3H) showing 13 binding pockets; only pockets ranked 1 and 2 showed the highest results regarding score (30.22, 28.81), probability (0.918, 0.910), residue number (27, 28) and conservation (0.743, 0.717) for pockets 1 and 2, respectively. Visualization showed the high-confident regions of the structure (score >0.070) colored as per pocket ranking.

Table 2 *In vitro* anti-Alzheimer activities of the hydroalcoholic extracts prepared from the different organs of *Ochrosia elliptica* Labill.

Hydroalcoholic extract of *Ochrosia elliptica* Labill.	IC_{50} (μg mL^{-1})	
	AChE	BChE
Stems	25.37 ± 0.69	48.01 ± 0.12
Barks	18.24 ± 1.66	35.77 ± 1.34
Roots	16.11 ± 0.79	35.39 ± 0.52
Fruits	12.77 ± 0.24	29.98 ± 0.51
Donepezil	0.23 ± 0.03	0.31 ± 0.0033

Table 3 Prediction results by PrankWeb on the binding pockets of AChE (PDB ID: 7E3H)

Rank↑	Score	Probability	# of residues	Avg conservation	Residues pocket 1 7E3H
1	30.22	0.918	27	0.743	A_120 A_121 A_122 A_124 A_125 A_126 A_133 A_202 A_203 A_286 A_289 A_293 A_294 A_295 A_296 A_297 A_337 A_338 A_341 A_447 A_72 A_74 A_75 A_76 A_83 A_86 A_87
2	28.81	0.91	28	0.717	
3	2.8	0.087	10	0.086	
4	2.72	0.083	10	0.086	
5	2.63	0.078	9	0.108	
6	1.97	0.04	12	0	
7	1.95	0.04	11	1.743	
8	1.88	0.036	10	0	
9	1.8	0.033	12	0.081	
10	1.51	0.021	12	0	
11	1.3	0.014	12	0	
12	1.24	0.013	8	0.749	
13	1.23	0.013	8	0.883	

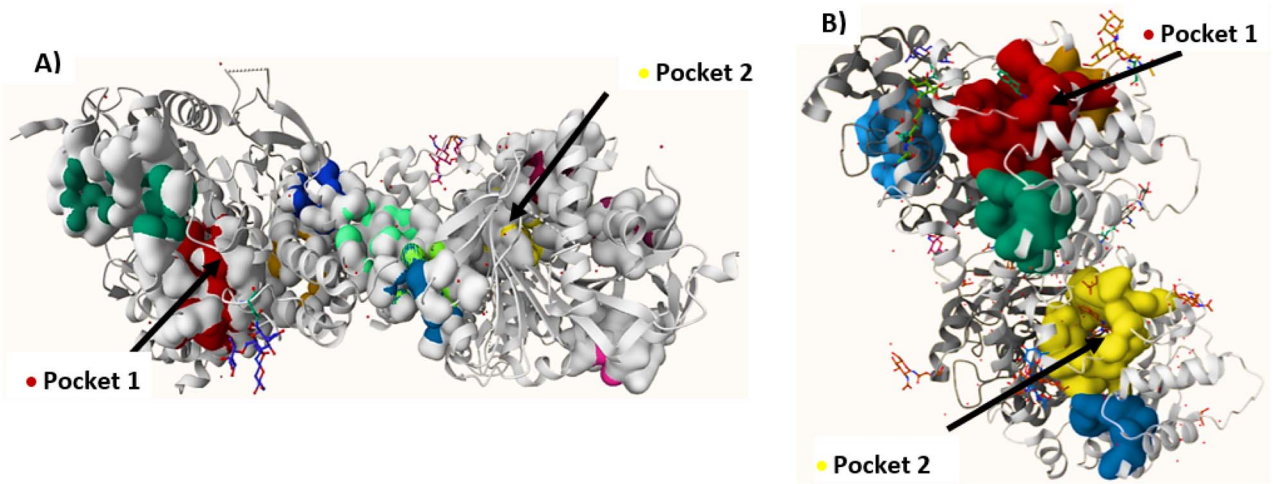

Fig. 2 PrankWeb predictions of small-molecule binding pockets of (A) AChE (PDB ID: 7E3H) (pockets 1–13) and (B) BChE (PDB ID: 4TPK) (pockets 1–6) with the ranking color code highlighting mainly pockets 1 (red) and 2 (yellow).

Pocket 1 was suspected to be the most predictable binding pocket for small molecules binding *via* interaction with the identified amino acid residues (Fig. 2).

Furthermore, Prank Web prediction results for BChE (PDB ID: 4TPK) showed 6 binding pockets, from which pockets that ranked 1 and 2 were the best based on score results (29.97, 27.62), probability (0.916, 0.903), residue number (25, 26) and conservation average (0.869, 0.813), respectively (Table 4). Visualization results suggested pocket 1 to be the most predictable ligand binding pocket based on the essential amino acid residues' interactions (Fig. 2).

Table 4 Prediction results by PrankWeb on binding pockets of BChE (PDB ID: 4TPK)

Rank↑	Score	Probability	# of residues	Avg conservation	Residues pocket 1 7E3H
1	29.97	0.916	25	0.869	A_115 A_116 A_117 A_119 A_120 A_121 A_125 A_128 A_197 A_198 A_231 A_285 A_286 A_287 A_288 A_328 A_329 A_332 A_398 A_430 A_438 A_439 A_440 A_70 A_82
2	27.62	0.903	26	0.813	
3	1.70	0.028	11	0.061	
4	1.05	0.008	10	2.045	
5	0.89	0.005	9	0.163	
6	0.87	0.004	9	0.160	

The DeepSite Web server prediction results revealed only four predicted pockets for AChE protein (PDB ID: 7E3H) for either chain A or B. However, the prediction results of BChE (PDB ID: 4TPK) showed 3 binding pockets when testing chain A and 4 binding pockets for chain B prediction. The visualization of the results showed that pocket 1 in either 7E3H or 4TPK proteins confirmed the best results, and although chain A confirmed some binding interactions with the key amino acid residues, the number of binding interactions with most of the essential amino acid residues for chain B exceeded that of chain A in both targets. In AChE pocket 1, interactions with TYR 72 and PHE 338 were observed during chain A prediction, and interactions with Phe295, Phe297, Trp86, Ser293, Ser125 and Tyr72 were observed after testing chain B (Fig. 3).

Moreover, the visualization of 4TPK chain A DeepSite Web server prediction showed that pocket 1 confirmed binding interactions with Trp82, Phe329, His438, and Ser287, and chain B showed Trp82, Asp70, Ser72, Tyr332, Phe329, and Ser287 interactions (Fig. 3).

Findings revealed that PrankWeb predictions showed more possible regions in both tested targets compared to DeepSite, where 7E3H showed 13 predicted binding pockets by PrankWeb compared to only 4 by DeepSite and 4TPK showed 6 by PrankWeb compared to only 3 predicted binding regions by DeepSite, with common predicted amino acid residues by both servers. These analyses confirmed that the PrankWeb results are more likely to be more valid giving more accurately identified predictions, as reported previously[54] (Fig. 4, Tables 3 and 4).

CAVER Web 1.0 tool (**https://loschmidt.chemi.muni.cz/caverweb/**) was used for further confirmation of the binding sites of the two mentioned targeted proteins. The CAVER Web tool was used for quantum tunneling of the best pose of each of the two active binding sites; from the 32 and 14 pockets predicted by CAVER for AChE (7E3H) and BChE (4TPK), respectively, the best six score ranked pockets are illustrated in Fig. 4. For quantum tunneling of the best pose, the results were measured and ranked according to the investigated priority scores for the four tunnels of AChE: (0.0920–0.900), with radius and length dimensions of the best tunnel priority, tunnel 1 of 2.249 Å and 3.896 6 Å, respectively. Furthermore, the results of BChE showed 11 tunnels (0.138–0.930) and tunnel 1 showing the best score revealed a radius and length of 3.646 Å and 8.733 Å, respectively (Fig. 5 and 6). The results showed that tunnel 1 was of the highest radius during the investigation of both enzymes. This plays an important role in

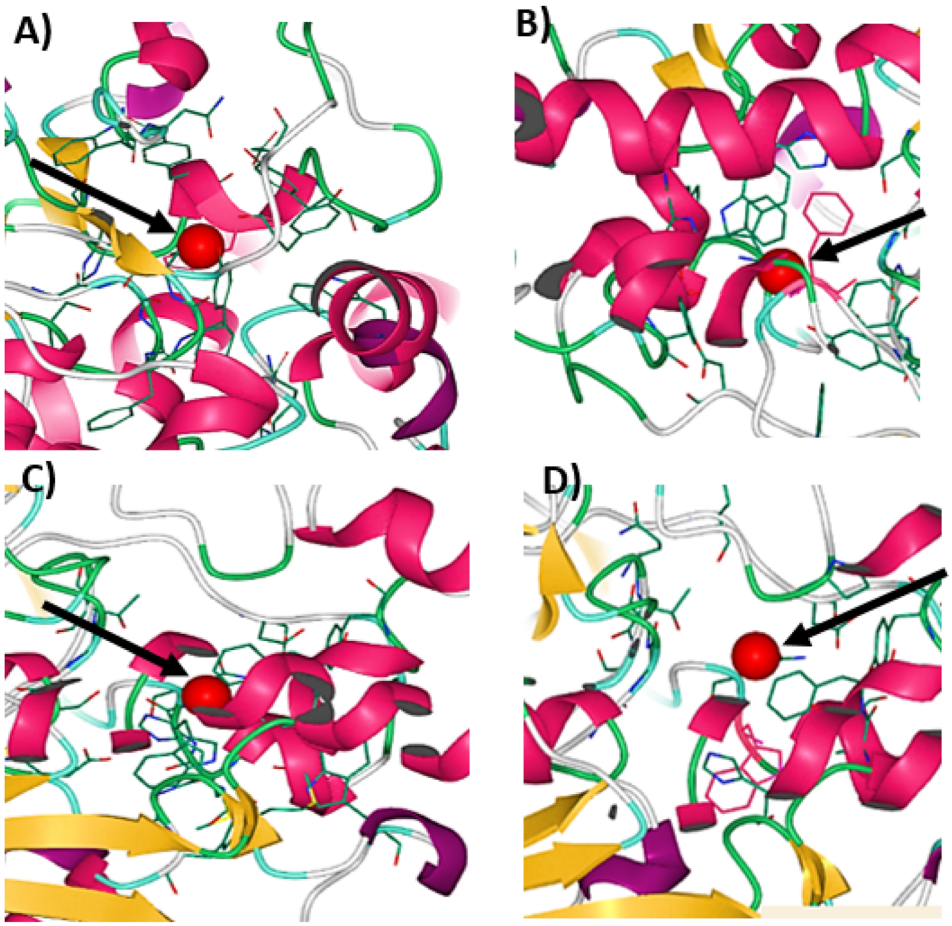

Fig. 3 DeepSite predictions showing binding pocket 1 (sited as red sphere) of (A) AChE (PDB ID: 7E3H) chain A prediction, (B) AChE (PDB ID: 7E3H) chain B prediction and (C) BChE (PDB ID: 4TPK) chain A prediction and (D) BChE (PDB ID: 4TPK) chain B prediction.

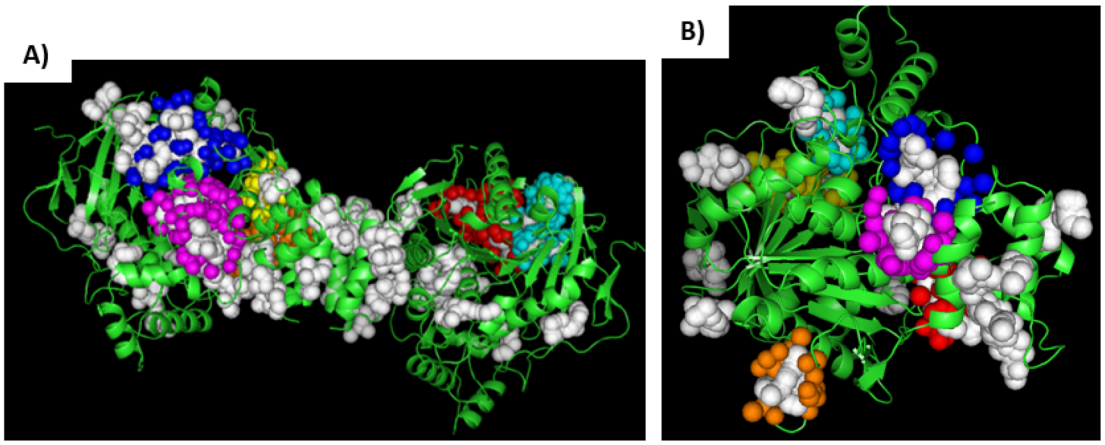

Fig. 4 Best score predicted protein pockets for (A) AChE (PDB ID: 7E3H) (pockets 1–6 out of 32 pockets: magenta, blue, red, yellow, orange, and cyan) and (B) BChE (PDB ID: 4TPK) (pockets 1–6 out of 14 pockets: red, magenta, yellow, blue, orange, and cyan) using CAVER Web 1.0 tools, viewed using PyMol.

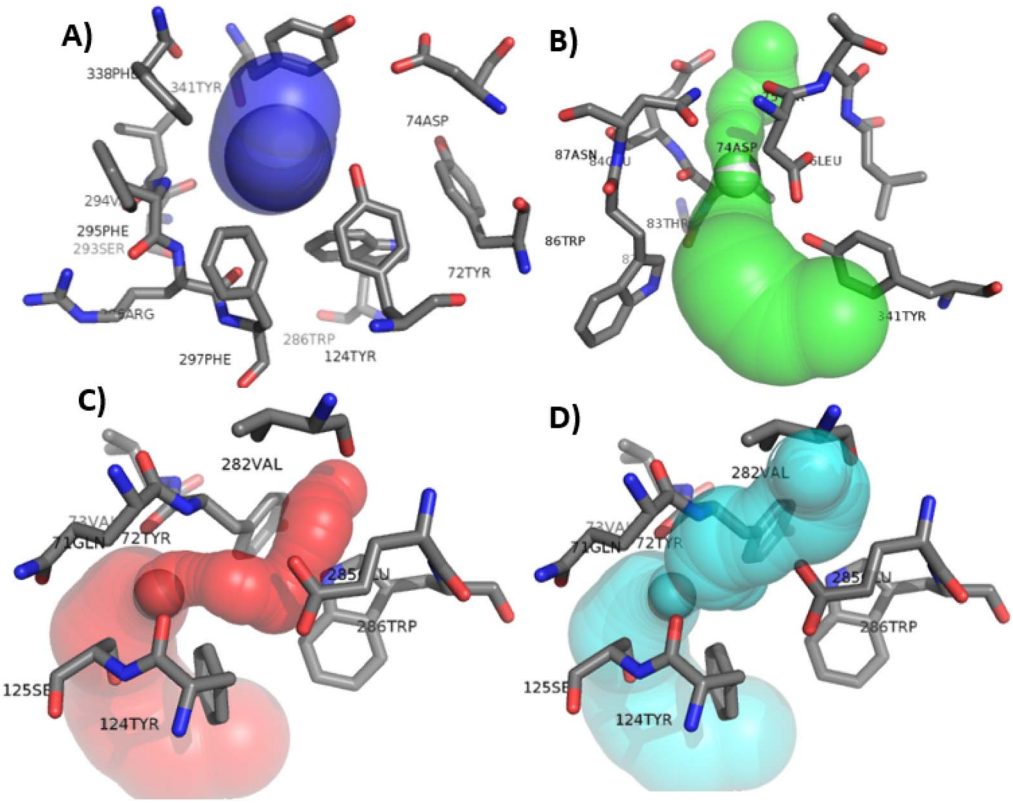

Fig. 5 Four predicted protein tunnels for 7E3H using CAVER Web 1.0 tools: (A) tunnel 1 (priority: 0.90), (B) tunnel 2 (priority: 0.50), (C) tunnel 3 (priority: 0.27) and (D) tunnel 4 (priority: 0.09).

predicting the ligand dimensions such as width, height or length as fitting requirements within the binding pocket.[54]

3.4. Molecular docking study

All the compounds were docked into the two target proteins AChE (PDB ID: 7E3H) and BChE (PDB ID: 4TPK) using C-Docker protocol. Fig. 7 shows the 2D-diagram of the docking results of the two ligands, with a (–)C-Docker interaction energy of donepezil of 57.72 (kcal mol^{-1}), and of *N*-((1-(2,3-dihydro-1*H*-inden-2-yl)piperidin-3-yl)methyl)-*N*-(2-methoxyethyl)-2-naphthamide as 47.71 (kcal mol^{-1}) on AChE and BChE, respectively, while (–)C-Docker interaction of the tested compounds lied within the range of 30.17–86.73 (kcal mol^{-1}) for AChE and 26.81–72.42 (kcal mol^{-1}) for BChE.

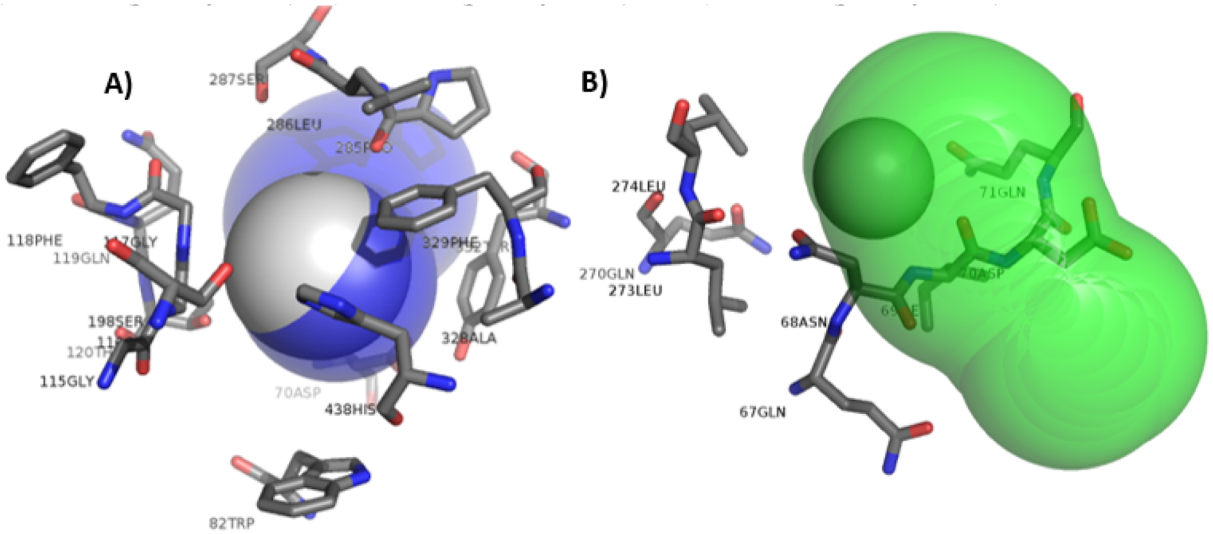

Fig. 6 The best 2 predicted protein tunnels (2 out of 11) for 4TPK using CAVER Web 1.0 tools: (A) tunnel 1 (priority: 0.93) and (B) tunnel 2 (priority: 0.83).

All the docked compounds (41 compounds) showed good interaction results with AChE (PDB ID: 7E3H), where most of the compounds showed comparable binding interactions at the active pocket to that of donepezil with stable (–)C-Docker interaction energy values, where 17 tested compounds revealed (–)C-Docker interaction energy values exceeding 50 kcal mol^{-1} compared to donepezil (E = −57.72 kcal mol^{-1}). Upon further filtration, it was observed that five compounds showed better interaction energy than that of the ligand as follows: compound **12** showed the best binding results (E = −86.73 kcal mol^{-1}), showing one hydrogen bond (H bond) with Phe295, Phe338, Gln291, Gly120, Asp74, Thr75, Tyr124, Tyr133, and Trp86 and two H bonds with Ser293, a hydrophobic bond with Phe338, Tyr337, Tyr341 and Trp286. Compound **13** (E = −63.22 kcal mol^{-1}) showed a H bond with Phe338, Asn87, Tyr341, and His447 and 2H bonds with Glu202. Moreover, carbon–hydrogen (C–H) interaction with Asp74 and van der Waals interaction with Ty72. Compound **16** (E =

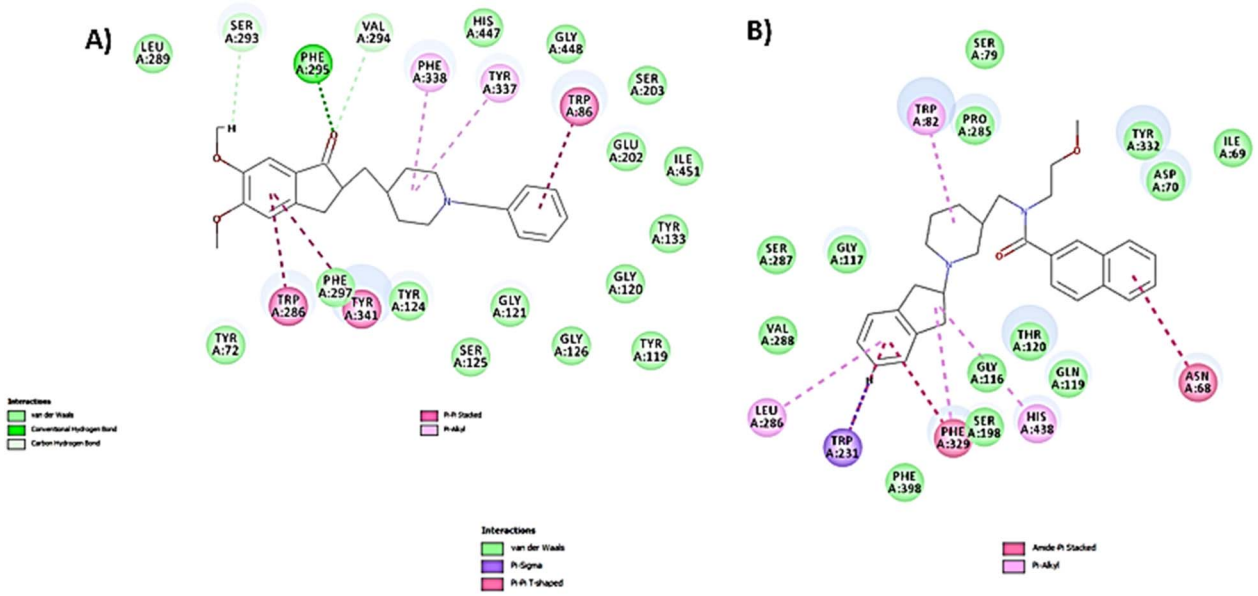

Fig. 7 2D diagram showing docking interactions of the ligands with the key amino acid residues at binding pockets: (A) donepezil with AChE (PDB ID: 7E3H), (E = −57.72 kcal mol^{-1}): hydrogen bond with Phe295; hydrophobic bond with Phe338, Tyr337, Tyr341, Trp86, Trp286 and Ser293. (B) *N*-((1-(2,3-Dihydro-1*H*-inden-2-yl)piperidin-3-yl)methyl)-*N*-(2-methoxyethyl)-2-naphthamide with BChE (PDB ID: 4TPK), (E = −47.71 kcal mol^{-1}): hydrophobic bonds with Phe329, His438, Trp82, Trp231, Asn68 and Leu286. Color code of dotted lines: green for H bonds, pink for Pi–alkyl bonds, purple for Pi–Pi bonding, and pale greenish for van der Waals interactions.

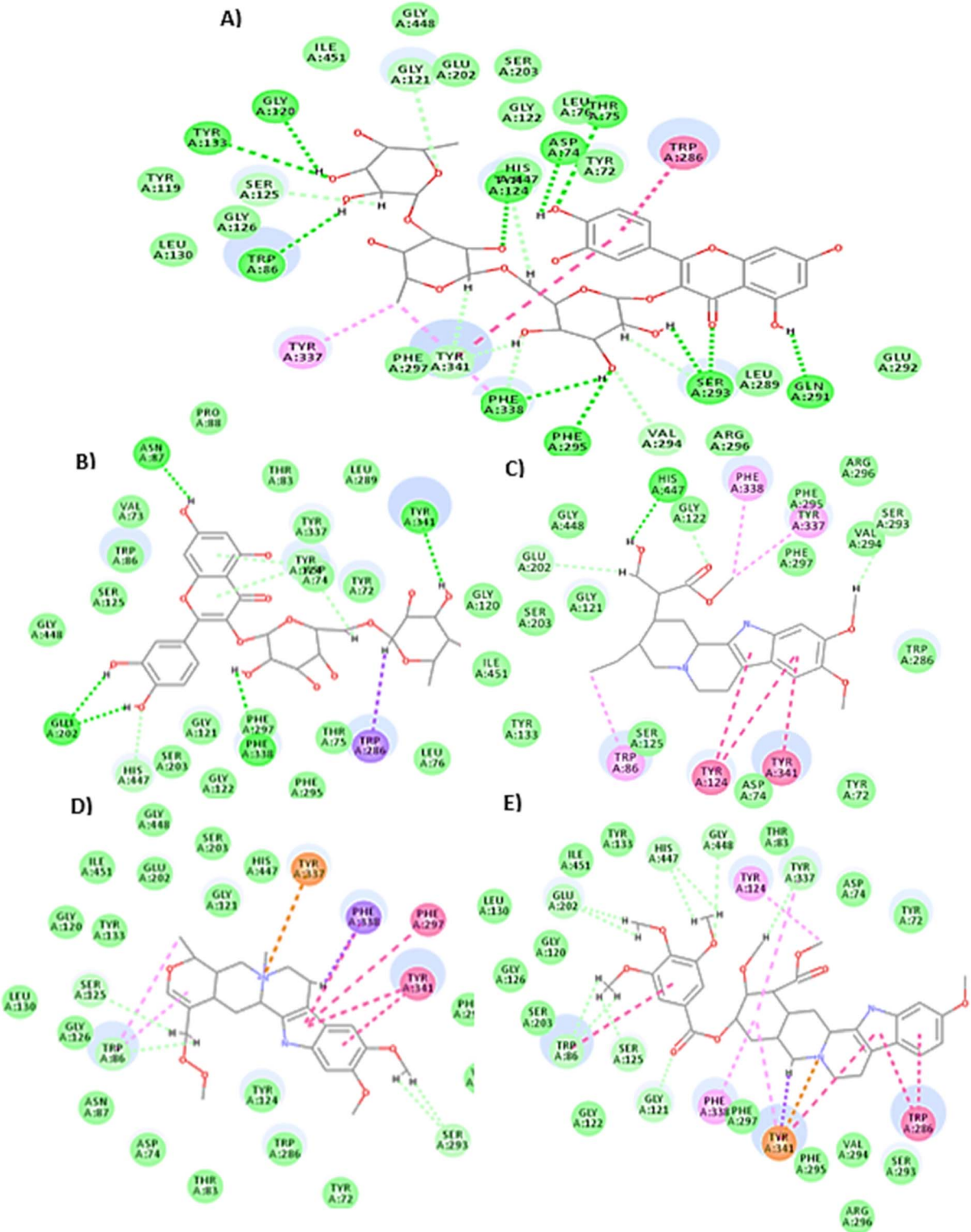

Fig. 8 2D interaction diagram of the best ligands after docking on AChE (PDB ID: 7E3H): (A) compound (**12**) (E = −86.73 kcal mol^{-1}), (B) compound (**13**) (E = −63.22 kcal mol^{-1}), (C) compound (**16**) (E = −59.64 kcal mol^{-1}), (D) compound (**30**) (E = −58.31 kcal mol^{-1}), and (E) compound (**40**) (E = −67.22 kcal mol^{-1}).

−59.64 kcal mol^{-1}) showed a H bond with His447, Gly122, and Val294 and a hydrophobic bond with Phe338, Tyr124, Tyr337, Tyr341 and Trp86. Compound **30** (E = −58.31 kcal mol^{-1}) showed a hydrophobic bond with Phe338, Phe297, Tyr341 and Trp86 and a C–H bond with Trp86, Ser293, and Ser125. In addition to Pi carbon interaction with Tyr337, compound **40** (E

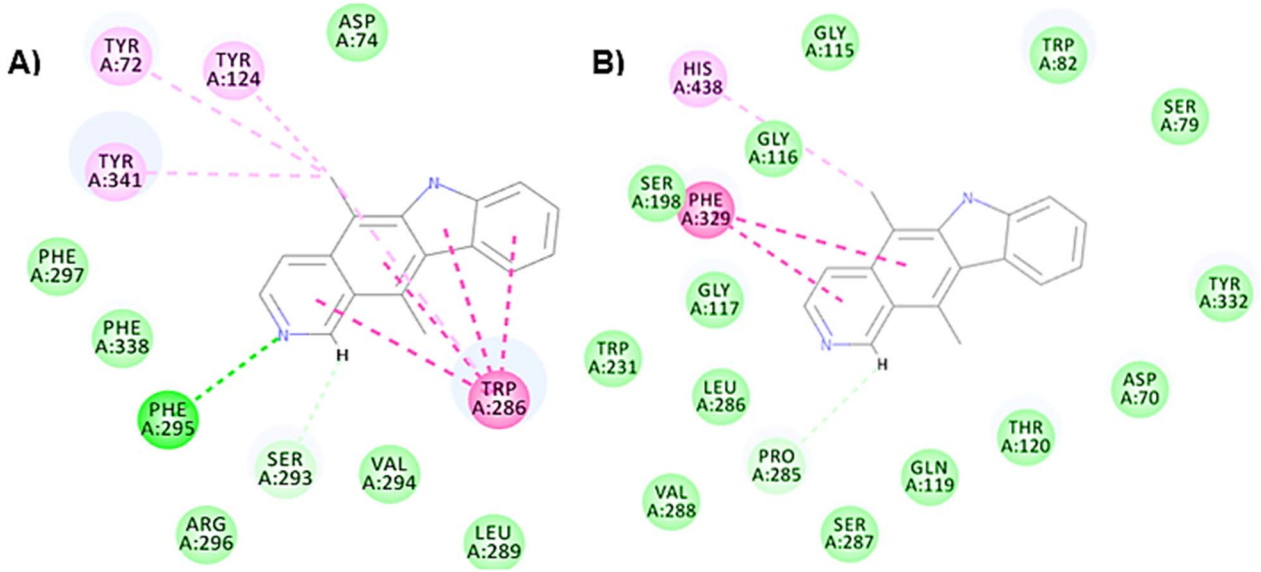

Fig. 9 2D interaction diagram of the least stable compound (compound **35**) after docking on (A) AChE (PDB ID: 7E3H) ($E = -30.17$ kcal mol^{-1}) and (B) BChE (PDB ID: 4TPK) ($E = -26.81$ kcal mol^{-1}), showing good interactions on both targets.

$= -67.22$ kcal mol^{-1}) showed a hydrophobic bond with Phe338, Tyr124, Tyr337, Tyr331, Tyr34, Trp86 and Trp286 and a C–H bond with Gly448, Glu202, His447, Ser125, and Tyr337. In addition, there was a Pi carbon interaction with Tyr337 (Fig. 8).

Furthermore, only six compounds showed (–)C-Docker interaction energy values less than 40 kcal mol^{-1}. Although these compounds revealed lower stability interaction energy values, their visual inspection confirmed good interactions at the binding site with the essential amino acid residues as follows: compound **17** ($E = -37.93$ kcal mol^{-1}), compound **31** ($E = -38.10$ kcal mol^{-1}), and compound **34** ($E = -36.69$ kcal mol^{-1}) showing a H bond with Phe 338, compound **35** ($E = -30.17$ kcal mol^{-1}) confirmed a H bond with Phe 295, compound **36** ($E = -32.88$ kcal mol^{-1}), compound **37** ($E = -38.67$ kcal mol^{-1}) and compound **38** ($E = -37.38$ kcal mol^{-1}). Fig. 9 presents compound **35** which showed the least stability results, yet with comparable binding interactions at the binding pockets of both AChE (PDB ID: 7E3H) and BChE (PDB ID: 4TPK).

While checking the BChE target (PDB ID: 4TPK) docking results, it was observed that most of the compounds showed promising results. Ten compounds out of 41 docked compounds showed more stable C-Docker interaction energy than the re-docked ligand ($E = -47.71$ kcal mol^{-1}), as follows: compound **10** ($E = -53.41$ kcal mol^{-1}), compound **12** ($E = -72.42$ kcal mol^{-1}), compound **13** ($E = -68.66$ kcal mol^{-1}), compound **14** ($E = -49.58$ kcal mol^{-1}), compound **15** ($E = -59.78$ kcal mol^{-1}), compound **16** ($E = -50.79$ kcal mol^{-1}), compound **24** ($E = -49.01$ kcal mol^{-1}), compound **27** ($E = -51.32$ kcal mol^{-1}), compound **30** ($E = -50.34$ kcal mol^{-1}), compound **40** ($E = -69.02$ kcal mol^{-1}), and compound **41** ($E = -66.03$ kcal mol^{-1}), which were visualized, revealing good interactions at the binding site. It was observed that the five best docked compounds (compounds **12**, **13**, **16**, **30** and **40**) against AChE (PDB ID: 7E3H) were also superior while targeting BChE (PDB ID: 4TPK), confirming the essential binding interactions with amino acid residues in the active pockets (Fig. 10).

Based on the docking results, it was observed that compound **12** could be considered as the most promising compound, confirming the essential binding interactions on the two studied targets with the best docking interaction energy compared to all the docked compounds and the ligands. The overlay visualization of compound **12** with each of the two ligands in the two active sites of the two studied enzymes showed good fitting with the neighboring amino acid residues, which suggested promising biological interactions at the binding sites (Fig. 11). These results encouraged further study applying dynamic simulation studies to determine the stability of the two studied enzymes AChE and BChE after docking.

Moreover, the visualization of the molecular fitting of compound **12** on both enzymes after using the CAVER Web 1.0 tool showed good fitting within the best score-ranked 4 tunnels. It is worth noting that the tunnel dimensions hinge on variables either being dependent or independent, and the protein radius is essential to calculate the needed ligand's fitting dimensions in order to achieve the best biological results (Fig. 12).

3.5. Standard dynamic simulations

Discovery Studio 4.0 was used to investigate the stability of both proteins: AChE and BChE, and the produced conformations after their docking *via* standard dynamic simulation were analyzed through trajectory studies. The stability of the most promising docked compound (**12**) was compared to the free states of the two enzymes AChE and BChE. The stability was determined as the total energy plot against the time and calculation of root mean square fluctuations (RMSFs) against the produced conformations. The free state of AChE (7E3H) and

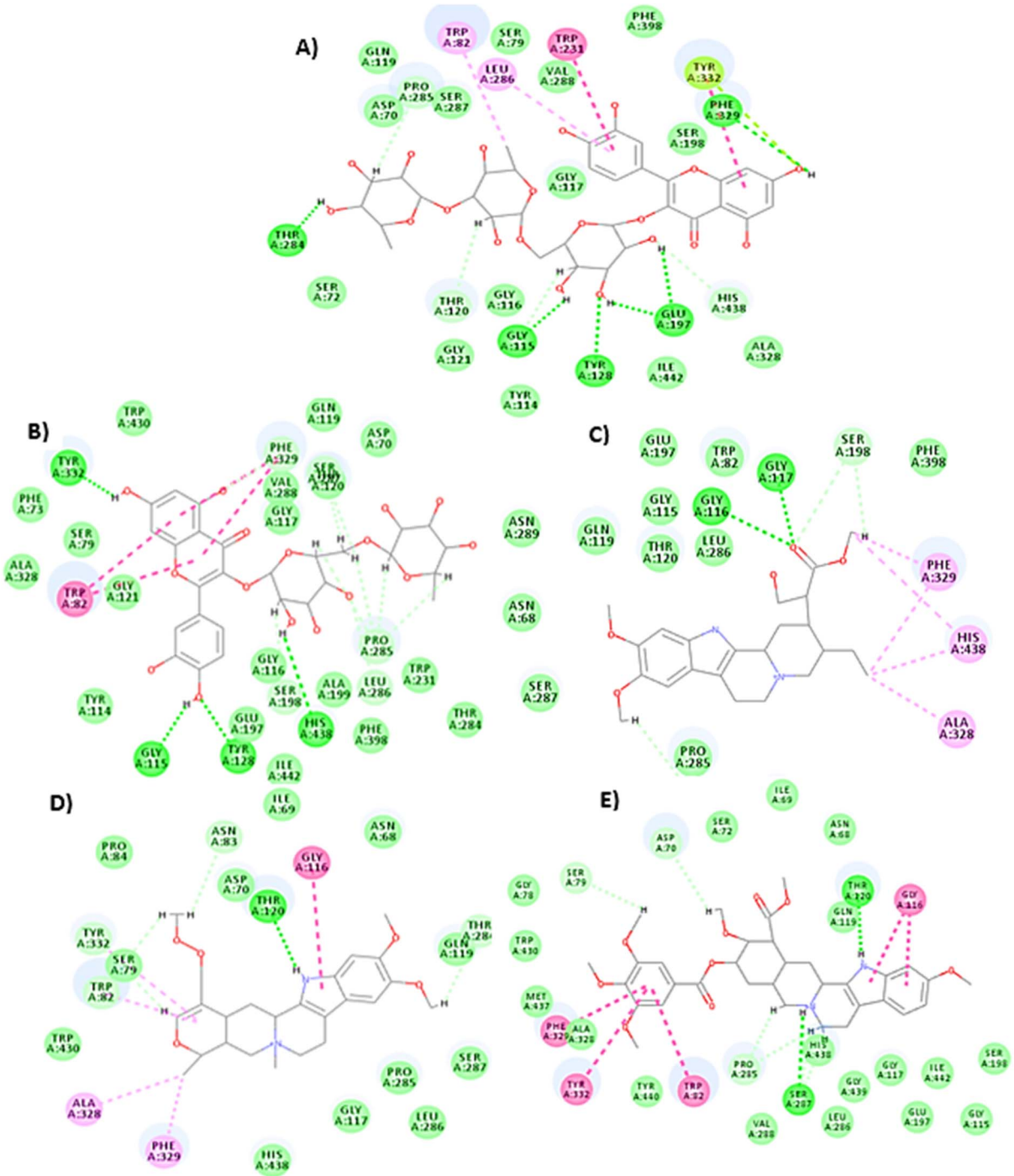

Fig. 10 2D interaction diagram of the five most promising ligands after docking on BChE (PDB ID: 4TPK): (A) compound (**12**) (E = −72.42 kcal mol^{-1}), (B) compound (**13**) (E = −68.66 kcal mol^{-1}), (C) compound (**16**) (E = −50.79 kcal mol^{-1}), (D) compound (**30**) (E = −50.34 kcal mol^{-1}), and (E) compound (**40**) (E = −69.02 kcal mol^{-1}).

BChE (4TPK) showed a decrease in total energy *versus* time; it is obvious that, among the same time frame, the docked enzymes with compound **12** also showed a total energy decrease (Fig. 13), which could be explained as similar behaviors conducted after docking by compound **12** being of high stability compared to the two enzymes in their free states.

The values of RMSFs of AChE (7E3H) in its free state lied in the 0.25–4.5 range, while after being docked with compound **12**, the RMSF values were: 0.25–4.0, revealing stable fluctuations over time. The same for BChE (4TPK): the RMSF values of the free protein showed a range of 0.5–7.5, and for the docked state with compound **12**, the range was 0.50–4.75, showing high stability (Fig. 14).

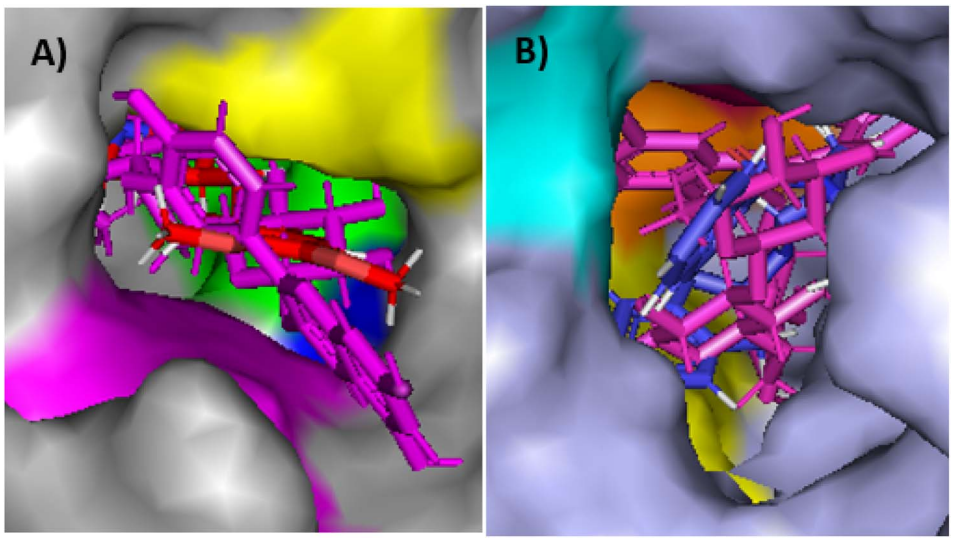

Fig. 11 Overlay of the ligand and compound **12** in the active sites of (A) AChE protein (7E3H) (gray), ligand (red), compound **12** (magenta), Phe295 (blue), Phe338 (green), Trp286 (magenta), His447 (green), tyr341 (yellow). (B) BChE protein (4TPK) (bluish grey), ligand (blue), compound **12** (magenta), Trp82 (yellow), Phe329 (pink), His438 (orange) visualized using Pymol.

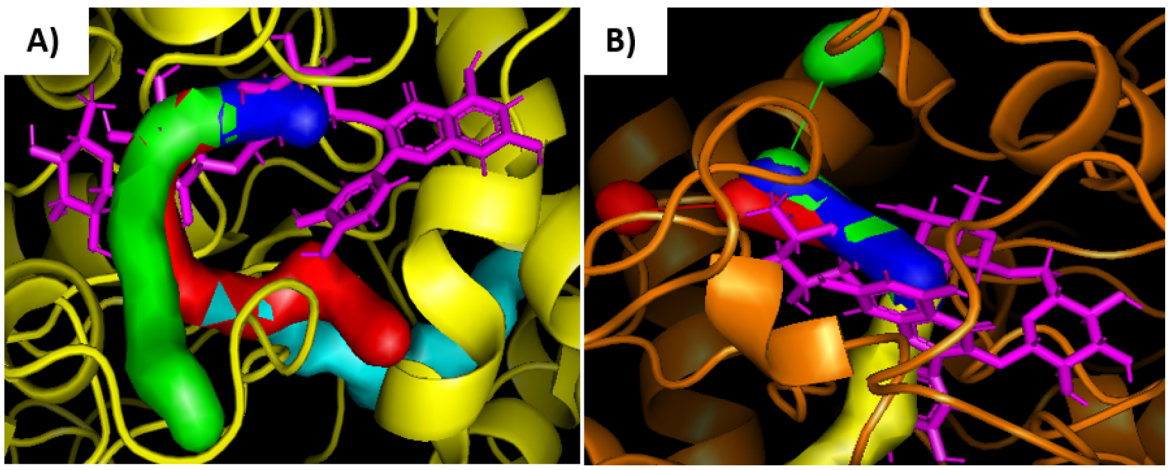

Fig. 12 The best 4 predicted protein tunnels with compound **12** (magenta) using CAVER Web 1.0 tools: (A) 7E3H (yellow) and tunnels 1–4 (blue, green, red and cyan, respectively); (B) 4TPK (orange) and tunnels 1–4 (blue, green, red and yellow, respectively), viewed using PyMol.

3.6. Biological activity prediction

The predicted biological activity of the most promising compound (**12**) targeting different proteins was performed using PASS Online Way2Drug **https://www.way2drug.com/passtargets/**, by uploading the 2D ChemBioDraw chemical structure of the compound. The results indicated the activity against muscarinic acetylcholine receptor M1 (ChEMBL id: CHEMBL216) with 0.2819 confidence value, and activity against acetylcholinesterase (ChEMBL id: CHEMBL220) with a maximum confidence of 0.1483.[56] The cellular and molecular mechanisms of the quercetin and its derivatives involved in the protection against AD were highly documented in previous works, which are mainly due to their anti-inflammatory and antioxidant actions.[79] Furthermore, quercetin derivatives have relevance to the Alzheimer's disease (AD) pathogenesis cascade and demonstrate the ability to protect neuronal cells from oxidative stress-induced damage.[77,80] In addition, flavonoids such as quercetin of **12** and **13** exhibited multiple mechanisms of action that are involved in the pathogenesis of AD including AChE inhibition, antioxidant, neuroprotection, and anti-Aβ aggregation. In addition, quercitrin exhibited antioxidant and anti-hyaluronidase properties.[81] Consequently, flavonoid-rich nutraceuticals may represent a cost-effective treatment option for AD, but additional well-designed, randomized, and placebo-controlled clinical trials are necessary to evaluate their optimal dosages, effectiveness, and long-term safety in humans.[82]

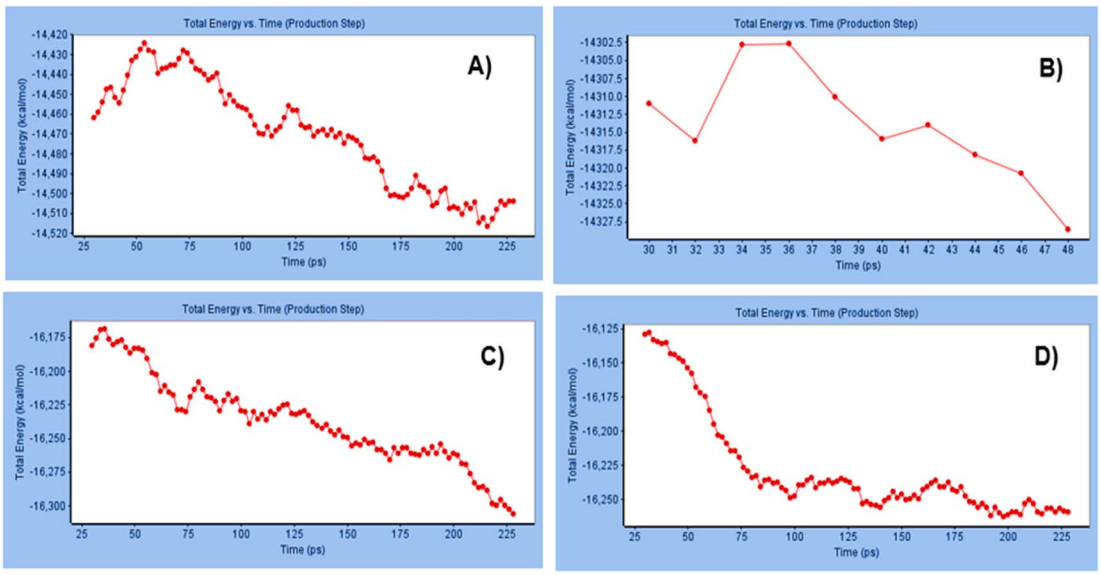

Fig. 13 Dynamic simulation study results represented by the total energy *versus* time plot in the production step: (A) AChE (PDB ID: 7E3H) in its free state before docking, (B) AChE after docking with compound **12**, (C) BChE (PDB ID: 4TPK) in its free state before docking and (D) BChE after docking with compound **12**.

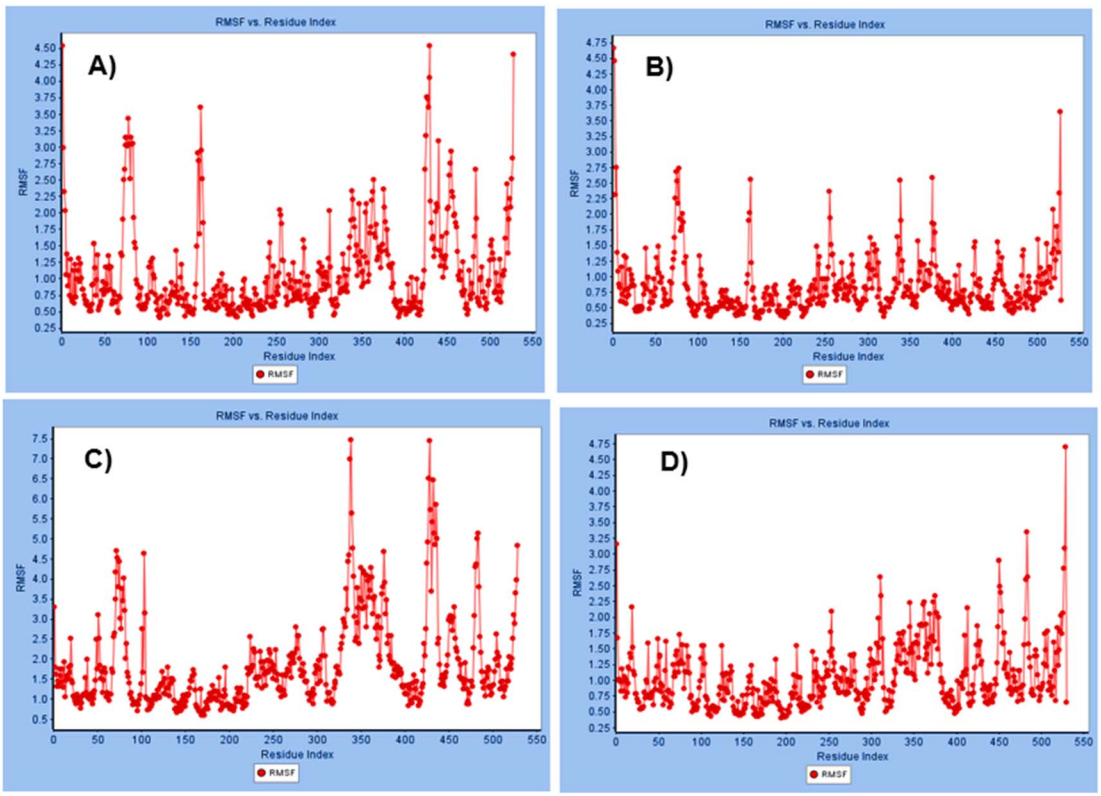

Fig. 14 Analyzed trajectory study results represented by the RMSF *versus* residue index plot of: (A) AChE (PDB ID: 7E3H) in its free state before docking, (B) AChE after docking with compound **12**, (C) BChE (PDB ID: 4TPK) in its free state before docking and (D) BChE after docking with compound **12**.

4 Conclusions

A total of 39 Apocynaceae alkaloids were tentatively identified based on the UPLC-MS/MS analysis of different parts of *O. elliptica*. The major bioactive metabolites were docked against both AChE and BChE target enzymes and reflected a good potential as anti-Alzheimer therapies with good binding scores and comparable binding modes at the binding pockets compared to the downloaded ligands; furthermore, a dynamic simulation study was conducted on the most predicted active compound quercetin-3-*O*-rhamnosyl-(1-3)-rhamnosyl-(1-6)-hexoside and confirmed good stability results compared to the free state proteins. Future work could progress towards implementing this strategy to identify novel derivatives isolated from *Ochrosia* plants as targets for AD.

List of abbreviations

AChE	Acetylcholinesterase
AD	Alzheimer's disease
Aβ	Amyloid plaques
BChE	Butyrylcholinesterase
DTNB	Dithio-bis-(2-nitrobenzoic acid)
ESI	Electrospray ionization
FDA	Food and drug administration
NFTs	Neurofibrillary tangles
RMSFs	Root-mean-square fluctuations
UPLC-MS/MS	Ultra-performance liquid chromatography coupled with tandem mass spectrometry

Data availability

The data supporting the findings of this study are available within the article.

Author contributions

Conceptualization: M. A. S., R. A. E., and E. A. S.; data curation: A. A. M., M. A. S., and R. A. E.; resources: M. A. S., A. A. M., and R. A. E.; investigation: A. A. M., M. A. S., and R. A. E.; analysis: A. A. M., M. A. S., and R. A. E.; writing – original draft; writing, review, and editing: all the authors. All the authors have read and agreed to the published version of the manuscript.

Conflicts of interest

The authors declare no competing interests.

Acknowledgements

This research received no external funding.

References

1 M. Citron, Alzheimer's disease: strategies for disease modification, *Nat. Rev. Drug Discovery*, 2010, **9**, 387–398.
2 A. F. Kassem, M. A. Omar, A. Temirak, R. A. El-Shiekh and A. M. Srour, Barbiturate–sulfonate hybrids as potent cholinesterase inhibitors: design, synthesis and molecular modeling studies, *Future Med. Chem.*, 2024, 1–17.
3 R. A. El-Shiekh, H. A. Kassem, A. E. Khaleel and M. M. Abd El-Mageed, Anticholinesterases activity of Murraya koenigii (L.) Spreng. and Murraya paniculata (L.) Jacq. essential oils with GC/MS analysis and molecular docking, *Nat. Prod. Res.*, 2024, **38**, 2155–2159.
4 R. M. Ibrahim, R. A. El-Shiekh, O. G. Mohamed, A. A. Al-Karmalawy, A. Tripathi and P. M. Abdel-Baki, LC/MS-Based Metabolomics Reveals Chemical Variations of Two Broccoli Varieties in Relation to Their Anticholinesterase Activity: In vitro and In silico Studies, *Plant Foods Hum. Nutr.*, 2024, 1–8.
5 P. Scheltens, K. Blennow, M. M. Breteler, B. De Strooper, G. B. Frisoni, S. Salloway, *et al.*, Alzheimer's disease, *Lancet*, 2016, **388**, 505–517.
6 M. A. Omar, R. A. El-Shiekh, D. H. Dawood, A. Temirak and A. M. Srour, Hydrazone–sulfonate hybrids as potential cholinesterase inhibitors: design, synthesis and molecular modeling simulation, *Future Med. Chem.*, 2023, **15**, 2269–2287.
7 M. H. Mahnashi, M. A. Alshahrani, M. H. Nahari, S. Su Hassan, M. S. Jan, M. Ayaz, *et al.*, In-vitro, in-vivo, molecular docking and ADMET studies of 2-substituted 3, 7-dihydroxy-4H-chromen-4-one for oxidative stress, inflammation and Alzheimer's disease, *Metabolites*, 2022, **12**, 1055.
8 J. D. Grill and J. L. Cummings, Current therapeutic targets for the treatment of Alzheimer's disease, *Expert Rev. Neurother.*, 2010, **10**, 711–728.
9 D. H. Dawood, A. M. Srour, M. A. Omar, T. A. Farghaly and R. A. El-Shiekh, Synthesis and molecular docking simulation of new benzimidazole–thiazole hybrids as cholinesterase inhibitors, *Arch. Pharm.*, 2024, **357**, 2300201.
10 M. A. Youssef, S. S. Panda, R. A. El-Shiekh, E. M. Shalaby, D. R. Aboshouk, W. Fayad, *et al.*, Synthesis and molecular modeling studies of cholinesterase inhibitor dispiro [indoline-3, 2′-pyrrolidine-3′, 3′′-pyrrolidines], *RSC Adv.*, 2020, **10**, 21830–21838.
11 A. A. Abduljawad, M. A. Elawad, M. E. M. Elkhalifa, A. Ahmed, A. A. E. Hamdoon, L. H. M. Salim, *et al.*, Alzheimer's disease as a major public health concern: Role of dietary saponins in mitigating neurodegenerative disorders and their underlying mechanisms, *Molecules*, 2022, **27**, 6804.
12 M. H. Mahnashi, M. Ashraf, A. H. Alhasaniah, H. Ullah, A. Zeb, M. Ghufran, *et al.*, Polyphenol-enriched Desmodium elegans DC. ameliorate scopolamine-induced amnesia in animal model of Alzheimer's disease: In Vitro, In Vivo and In Silico approaches, *Biomed. Pharmacother.*, 2023, **165**, 115144.
13 H. M. Hussein, E. Mohsen, A. R. Abdelmonem, M. A. Abdel Kawy, A. A. Al-Karmalawy and R. A. El-Shiekh, New Insight into the Anticholinesterase Potential of Cordia dichotoma G. Forst. and Cordia sebestena L. Leaves, Phenolic

Characterization of their Active Extracts by HPLC-DAD and Molecular Modeling, *Egypt. J. Chem.*, 2024, **67**, 225–237.

14 A. A. Hamed, R. A. El-Shiekh, O. G. Mohamed, E. A. Aboutabl, F. I. Fathy, G. A. Fawzy, *et al.*, Cholinesterase inhibitors from an endophytic fungus Aspergillus niveus Fv-er401: metabolomics, isolation and molecular docking, *Molecules*, 2023, **28**, 2559.

15 R. A. El-Shiekh, A. A. Shalabi, O. S. Al-Hawshabi, M. A. Salkini and E. Abdel-Sattar, Anticholinesterase and anti-inflammatory constituents from Caralluma awdeliana, a medicinal plant from Yemen, *Steroids*, 2023, **193**, 109198.

16 A. Agnihotri and O. I. Aruoma, Alzheimer's disease and Parkinson's disease: a nutritional toxicology perspective of the impact of oxidative stress, mitochondrial dysfunction, nutrigenomics and environmental chemicals, *J. Am. Coll. Nutr.*, 2020, **39**, 16–27.

17 R. A. El-Shiekh, D. A. Al-Mahdy, M. S. Hifnawy and E. A. Abdel-Sattar, Pharmacognostical study of Ochrosia elliptica Labill.(Apocynaceae), *J. Appl. Pharm. Sci.*, 2019, **9**, 049–057.

18 E. Abdel-Sattar and R. A. El-Shiekh, Chemical composition and biological activities of genus Ochrosia: a mini review, *Phytochem. Lett.*, 2024, **62**, 92–111.

19 Y.-H. Fua, Structurally diverse indole alkaloids from Ochrosia elliptica, *Heterocycles*, 2017, **94**, 743–749.

20 R. A. El-shiekh, D. A. Al-Mahdy, M. S. Hifnawy, T. Tzanova, E. Evain-Bana, S. Philippot, *et al.*, Chemical and biological investigation of Ochrosia elliptica Labill. cultivated in Egypt, *Rec. Nat. Prod.*, 2017, **11**, 552–557.

21 R. A. El-Shiekh, D. A. Al-Mahdy, M. S. Hifnawy and E. Abdel-Sattar, Biological and chemical assessment of Ochrosia elliptica Labill leaves, *Arabian J. Sci. Eng.*, 2021, **46**, 5247–5255.

22 R. Elshimy, W. Y. Khawagi, I. A. Naguib, S. I. Bukhari and R. A. El-Shiekh, 9-Methoxyellipticine: Antibacterial Bioactive Compound Isolated from Ochrosia elliptica Labill. Roots, *Metabolites*, 2023, **13**, 643.

23 R. M. Labib, F. Zulfiqar, M. A. Ibrahim, P. Balachandran, J. Zhang and S. A. Ross, FOXO signal activating alkaloids isolated from Ochrosia elliptica leaf cultivated in Egypt, *Med. Chem. Res.*, 2019, **28**, 1628–1632.

24 S. Mikutis, S. Lawrinowitz, C. Kretzer, L. Dunsmore, L. Sketeris, T. Rodrigues, *et al.*, Machine Learning Uncovers Natural Product Modulators of the 5-Lipoxygenase Pathway and Facilitates the Elucidation of Their Biological Mechanisms, *ACS Chem. Biol.*, 2023, **19**, 217–229.

25 F. Noor, M. Junaid, A. H. Almalki, M. Almaghrabi, S. Ghazanfar and M. Tahir ul Qamar, Deep learning pipeline for accelerating virtual screening in drug discovery, *Sci. Rep.*, 2024, **14**, 28321.

26 Y.-Q. Wang, L.-P. Hu, G.-M. Liu, D.-S. Zhang and H.-J. He, Evaluation of the nutritional quality of Chinese kale (Brassica alboglabra Bailey) using UHPLC-Quadrupole-Orbitrap MS/MS-based metabolomics, *Molecules*, 2017, **22**, 1262.

27 R. C. De Vos, S. Moco, A. Lommen, J. J. Keurentjes, R. J. Bino and R. D. Hall, Untargeted large-scale plant metabolomics using liquid chromatography coupled to mass spectrometry, *Nat. Protoc.*, 2007, **2**, 778–791.

28 M. Maldini, F. Natella, S. Baima, G. Morelli, C. Scaccini, J. Langridge, *et al.*, Untargeted metabolomics reveals predominant alterations in lipid metabolism following light exposure in broccoli sprouts, *Int. J. Mol. Sci.*, 2015, **16**, 13678–13691.

29 D. Lučić, I. Pavlović, L. Brkljačić, S. Bogdanović, V. Farkaš, A. Cedilak, *et al.*, Antioxidant and Antiproliferative Activities of Kale (Brassica oleracea L. Var. acephala DC.) and Wild Cabbage (Brassica incana Ten.) Polyphenolic Extracts, *Molecules*, 2023, **28**, 1840.

30 L. A. Barny, J. A. Tasca, H. A. Sanchez, C. R. Smith, S. Koptur, T. Livshultz, *et al.*, Chemotaxonomic investigation of Apocynaceae for retronecine-type pyrrolizidine alkaloids using HPLC-MS/MS, *Phytochemistry*, 2021, **185**, 112662.

31 P. Kumar, A. Bhushan, P. Gupta and S. Gairola, Comparative morpho-anatomical standardization and chemical profiling of root drugs for distinction of fourteen species of family Apocynaceae, *Bot. Stud.*, 2022, **63**, 12.

32 J. Liu, Y. Liu, Y.-j Pan, Y.-G. Zu and Z.-H. Tang, Determination of alkaloids in Catharanthus roseus and Vinca minor by high-performance liquid chromatography–tandem mass spectrometry, *Anal. Lett.*, 2016, **49**, 1143–1153.

33 A. A. Al-Karmalawy, R. Alnajjar, A. A. Elmaaty, F. A. Binjubair, S. T. Al-Rashood, B. S. Mansour, *et al.*, Investigating the promising SARS-CoV-2 main protease inhibitory activity of secoiridoids isolated from Jasminum humile; in silico and in virto assessments with structure-activity relationship, *J. Biomol. Struct. Dyn.*, 2023, 1–13.

34 K. I. Eissa, M. M. Kamel, L. W. Mohamed, A. S. Doghish, R. Alnajjar, A. A. Al-Karmalawy, *et al.*, Design, synthesis, and biological evaluation of thienopyrimidine derivatives as multifunctional agents against Alzheimer's disease, *Drug Dev. Res.*, 2023, 937–961.

35 A. Tripathi and K. Misra, Molecular docking: A structure-based drug designing approach, *JSM Chem.*, 2017, **5**, 1042–1047.

36 R. Nisar, S. Ahmad, K.-u-R. Khan, A. E. Sherif, F. Alasmari, A. F. Almuqati, *et al.*, Metabolic profiling by GC-MS, in vitro biological potential, and in silico molecular docking studies of Verbena officinalis, *Molecules*, 2022, **27**, 6685.

37 J. R. Christie, P. Lang, L. M. Zelko, D. A. Palma, M. Abdelrazek and S. A. Mattonen, Artificial intelligence in lung cancer: bridging the gap between computational power and clinical decision-making, *Can. Assoc. Radiol., J.*, 2021, **72**, 86–97.

38 Y. Wu, X. Su, J. Lu, M. Wu, S. Y. Yang, Y. Mai, *et al.*, In Vitro and in silico analysis of phytochemicals from fallopia dentatoalata as dual functional cholinesterase inhibitors for the treatment of Alzheimer's disease, *Front. Pharmacol*, 2022, **13**, 905708.

39 Y. Nicolet, O. Lockridge, P. Masson, J. C. Fontecilla-Camps and F. Nachon, Crystal structure of human

butyrylcholinesterase and of its complexes with substrate and products, *J. Biol. Chem.*, 2003, **278**, 41141–41147.

40 A. Martinez and A. Castro, Novel cholinesterase inhibitors as future effective drugs for the treatment of Alzheimer's disease, *Expert Opin. Invest. Drugs*, 2006, **15**, 1–12.

41 R. A. El-Shiekh, M. M. Okba, A. A. Mandour, O. Kutkat, R. Elshimy, H. A. Nagaty, *et al.*, Eucalyptus Oils Phytochemical Composition in Correlation with Their Newly Explored Anti-SARS-CoV-2 Potential: in Vitro and in Silico Approaches, *Plant Foods Hum. Nutr.*, 2024, 1–7.

42 R. A. El-Shiekh, R. Elshimy, A. A. Mandour, H. A. Kassem, A. E. Khaleel, S. Alseekh, *et al.*, Murraya koenigii (L.) Sprengel seeds and pericarps in relation to their chemical profiles: new approach for multidrug resistant Acinetobacter baumannii ventilator-associated pneumonia, *Appl. Biol. Chem.*, 2024, **67**, 1–19.

43 S. M. Mohamed, M. A. Shalaby, R. A. El-Shiekh, A. F. Bakr, M. M. Rashad, S. R. Emam, *et al.*, Vitis vinifera L. seed standardized extract; a promising therapeutic against metabolic syndrome induced by high-fat/high-carbohydrate diet and streptozotocin in rats, *S. Afr. J. Bot.*, 2024, **167**, 476–486.

44 R. A. El-Shiekh, R. Elshimy, A. A. Mandour, H. A. Kassem, A. E. Khaleel, S. Alseekh, *et al.*, Phytochemical characterisation of leaves and stems of Murraya koenigii (L.) Sprengel and Murraya paniculata (L.) Jack and their antibacterial activity against multidrug-resistant Acinetobacter baumannii bacterial infection, *Int. J. Food Sci. Technol.*, 2024, **59**(10), 7998–8010.

45 E. Abdel-Sattar, O. Kutkat, R. A. El-Shiekh, M. K. El-Ashrey and A. M. El Kerdawy, In Silico and In Vitro Screening of Some Pregnane Glycosides Isolated from Certain Caralluma Species as SARS-COV-2 Main Protease Inhibitors, *Chem. Biodiversity*, 2024, e202301786.

46 R. M. Merghany, M. A. Salem, S. M. Ezzat, S. F. Moustafa, S. A. El-Sawi and M. R. Meselhy, A comparative UPLC-orbitrap-MS-based metabolite profiling of three Pelargonium species cultivated in Egypt, *Sci. Rep.*, 2024, **14**, 22765.

47 H. Tsugawa, T. Cajka, T. Kind, Y. Ma, B. Higgins, K. Ikeda, *et al.*, MS-DIAL: data-independent MS/MS deconvolution for comprehensive metabolome analysis, *Nat. Methods*, 2015, **12**, 523–526.

48 H. M. Hussein, E. Mohsen, A. R. Abdelmonem, M. A. Abdel Kawy, A. A. Al-Karmalawy and R. A. El-Shiekh, New Insight into the Anticholinesterase Potential of Cordia dichotoma G. Forst. and Cordia sebestena L. Leaves, Phenolic Characterization of their Active Extracts by HPLC-DAD and Molecular Modeling, *Egypt. J. Chem.*, 2024, **67**(8), 225–237.

49 K. Dileep, K. Ihara, C. Mishima-Tsumagari, M. Kukimoto-Niino, M. Yonemochi, K. Hanada, *et al.*, Crystal structure of human acetylcholinesterase in complex with tacrine: Implications for drug discovery, *Int. J. Biol. Macromol.*, 2022, **210**, 172–181.

50 B. Brus, U. Kosak, S. Turk, A. Pislar, N. Coquelle, J. Kos, *et al.*, Discovery, biological evaluation, and crystal structure of a novel nanomolar selective butyrylcholinesterase inhibitor, *J. Med. Chem.*, 2014, **57**, 8167–8179.

51 K. Dileep, K. Ihara, C. Mishima-Tsumagari, M. Kukimoto-Niino, M. Yonemochi, K. Hanada, *et al.*, Crystal structure of human acetylcholinesterase in complex with tacrine: Implications for drug discovery, *Int. J. Biol. Macromol.*, 2022, **210**, 172–181.

52 B. Brus, U. Kosak, S. Turk, A. Pislar, N. Coquelle, J. Kos, *et al.*, Discovery, biological evaluation, and crystal structure of a novel nanomolar selective butyrylcholinesterase inhibitor, *J. Med. Chem.*, 2014, **57**, 8167–8179.

53 R. Krivák and D. Hoksza, P2Rank: machine learning based tool for rapid and accurate prediction of ligand binding sites from protein structure, *J. Cheminf.*, 2018, **10**, 1–12.

54 H. A. Oyewusi, R. A. Wahab, K. A. Akinyede, G. M. Albadrani, M. Q. Al-Ghadi, M. M. Abdel-Daim, *et al.*, Bioinformatics analysis and molecular dynamics simulations of azoreductases (AzrBmH2) from Bacillus megaterium H2 for the decolorization of commercial dyes, *Environ. Sci. Eur.*, 2024, **36**, 31.

55 A. A. Mandour, E. B. Elkaeed, M. Hagras, H. M. Refaat and N. S. Ismail, Virtual screening approach for the discovery of selective 5α-reductase type II inhibitors for benign prostatic hyperplasia treatment, *Future Med. Chem.*, 2023, **15**, 2149–2163.

56 Y. A. Elkhawas, H. A. Gad, M. M. AbdelRazek, A. A. Mandour, M. M. Bishr, N. M. Al Musayeib, *et al.*, LC-ESI-MS/MS-Based Comparative Metabolomic Study, Antioxidant and Antidiabetic Activities of Three Lobelia Species: Molecular Modeling and ADMET Study, *ACS Omega*, 2024, **9**(18), 20477–20487.

57 E. M. Azmy, I. F. Nassar, M. Hagras, I. M. Fawzy, M. Hegazy, M. M. Mokhtar, *et al.*, New indole derivatives as multitarget anti-Alzheimer's agents: synthesis, biological evaluation and molecular dynamics, *Future Med. Chem.*, 2023, **15**, 473–495.

58 E. M. Azmy, I. F. Nassar, M. Hagras, I. M. Fawzy, M. Hegazy, M. M. Mokhtar, *et al.*, New indole derivatives as multitarget anti-Alzheimer's agents: synthesis, biological evaluation and molecular dynamics, *Future Med. Chem.*, 2023, **15**, 473–495.

59 P. Benoin, R. Burnell and J. Medina, Alkaloids of Aspidosperma excelsum Benth, *Can. J. Chem.*, 1967, **45**, 725–730.

60 S. Sagi, B. Avula, Y.-H. Wang and I. A. Khan, Quantification and characterization of alkaloids from roots of Rauwolfia serpentina using ultra-high performance liquid chromatography-photo diode array-mass spectrometry, *Anal. Bioanal. Chem.*, 2016, **408**, 177–190.

61 A. Ahond, H. Fernandez, J. Moore, C. Poupat, V. Sanchez, P. Potier, *et al.*, Contribution to the study of Ochrosiineae: alkaloids from Ochrosia moorei, *J. Nat. Prod.*, 1981, **45**, 725–730.

62 S. Kumar, A. Singh, V. Bajpai, M. Srivastava, B. P. Singh and B. Kumar, Structural characterization of monoterpene indole alkaloids in ethanolic extracts of Rauwolfia species by liquid chromatography with quadrupole time-of-flight mass spectrometry, *J. Pharm. Anal.*, 2016, **6**, 363–373.

63 P. Perera, T. Van Beek and R. Verpoorte, 16 (S)-Hydroxy-16, 22-dihydroapparicine, a new alkaloid from the leaves of Tabernaemontana dichotoma, *J. Nat. Prod.*, 1984, **47**, 835–838.

64 B. J. Zhang, J. M. Yan, Z. K. Wu, Y. P. Liu, M. F. Bao, G. G. Cheng, *et al.*, Alkaloids from Ochrosia borbonica, *Helv. Chim. Acta*, 2013, **96**, 2288–2298.

65 J. Bruneton, T. Sevenet and A. Cavé, Alcaloïdes des ecorces d'ochrosia vieillardii, *Phytochemistry*, 1972, **11**, 3073–3075.

66 W. Yin, M. S. Kabir, Z. Wang, S. K. Rallapalli, J. Ma and J. M. Cook, Enantiospecific total synthesis of the important biogenetic intermediates along the ajmaline pathway,(+)-polyneuridine and (+)-polyneuridine aldehyde, as well as 16-epivellosimine and macusine A, *J. Org. Chem.*, 2010, **75**, 3339–3349.

67 P. Crooks and B. Robinson, The isolation and identification of (−)-apparicine from Tabernamontana cumminsii, *J. Pharm. Pharmacol.*, 1970, **22**, 799–800.

68 A. R. Carroll, R. Addepalli, G. Fechner, J. Smith, G. P. Guymer, P. I. Forster, *et al.*, Alkaloids from the Australian rainforest tree Ochrosia moorei, *J. Nat. Prod.*, 2008, **71**, 1063–1065.

69 R. R. Cardoso, R. O. Neto, C. T. dos Santos D'Almeida, T. P. do Nascimento, C. G. Pressete, L. Azevedo, *et al.*, Kombuchas from green and black teas have different phenolic profile, which impacts their antioxidant capacities, antibacterial and antiproliferative activities, *Food Res. Int.*, 2020, **128**, 108782.

70 X.-Q. Zheng, Y. Nie, Y. Gao, B. Huang, J.-H. Ye, J.-L. Lu, *et al.*, Screening the cultivar and processing factors based on the flavonoid profiles of dry teas using principal component analysis, *J. Food Compos. Anal.*, 2018, **67**, 29–37.

71 B. Sungthong, K. Sithon, P. Panyatip, S. Tadtong, N. Nunthaboot and P. Puthongking, Quantitative analysis and in silico molecular docking screening for acetylcholinesterase inhibitor and ADME prediction of coumarins and carbazole alkaloids from Clausena harmandiana, *Nat. Prod.*, 2022, **16**, 358–369.

72 P. Sadhukhan, S. Saha, S. Dutta, S. Mahalanobish and P. C. Sil, Nutraceuticals: An emerging therapeutic approach against the pathogenesis of Alzheimer's disease, *Pharmacol. Res.*, 2018, **129**, 100–114.

73 Y. R. Hassan, R. A. El-Shiekh, H. M. El Hefnawy and C. G. Michael, Irvingia gabonensis baill.(African Mango): A comprehensive review of its ethnopharmacological significance, unveiling its long-standing history and therapeutic potential, *J. Ethnopharmacol.*, 2024, 117942.

74 M. I. Morales-Rivera, R. Alemón-Medina, A. Martínez-Hernández, C. Contreras-Cubas, N. F. Altamirano-Bustamante, J. Gómez-Garduño, *et al.*, Exome Sequence Data of Eight SLC Transporters Reveal That SLC22A1 and SLC22A3 Variants Alter Metformin Pharmacokinetics and Glycemic Control, *Pharmaceuticals*, 2024, **17**, 1385.

75 J. Melrose, The potential of flavonoids and flavonoid metabolites in the treatment of neurodegenerative pathology in disorders of cognitive decline, *Antioxidants*, 2023, **12**, 663.

76 M. Al Amin, Z. Dehbia, M. H. Nafady, M. Zehravi, K. P. Kumar, M. A. Haque, *et al.*, Flavonoids and Alzheimer's disease: reviewing the evidence for neuroprotective potential, *Mol. Cell. Biochem.*, 2024, 1–31.

77 S. Kamiloglu, M. Tomas and E. Capanoglu, Dietary flavonols and O-glycosides, *Handbook of dietary phytochemicals*, 2019, pp. 1–40.

78 H. Hassan, *Neuroprotective and anti-inflammatory potentials of rutin in an in vitro model of Alzheimer's disease* 2024.

79 E. Zaplatic, M. Bule, S. Z. A. Shah, M. S. Uddin and K. Niaz, Molecular mechanisms underlying protective role of quercetin in attenuating Alzheimer's disease, *Life Sci.*, 2019, **224**, 109–119.

80 M. A. Mirza, S. Mahmood, A. R. Hilles, A. Ali, M. Z. Khan, S. A. A. Zaidi, *et al.*, Quercetin as a therapeutic product: evaluation of its pharmacological action and clinical applications—a review, *Pharmaceuticals*, 2023, **16**, 1631.

81 K. Plekratoke, P. Waiwut, C. Yenjai, O. Monthakantirat, P. Takomthong, N. Nualkaew, *et al.*, Multi-Target Actions of Flavonoid Derivatives from Mesua ferrea Linn Flower against Alzheimer's disease Pathogenesis, *Biomed. Sci. Clin. Med.*, 2023, **62**, 169–180.

82 S. M. Kothawade, H. S. Buttar, H. S. Tuli and G. Kaur, Therapeutic potential of flavonoids in the management of obesity-induced Alzheimer's disease: an overview of preclinical and clinical studies, *Naunyn-Schmiedeberg's Arch. Pharmacol.*, 2023, **396**, 2813–2830.